JBC Papers in Press. Published on March 12, 2018 as Manuscript M117.811190
The latest version is at http://www.jbc.org/cgi/doi/10.1074/jbc.M117.811190

The transpeptidase PbpA and non-canonical transglycosylase RodA of *Mycobacterium tuberculosis* play important roles in regulating bacterial cell lengths

Divya Arora[1], Yogesh Chawla[1], Basanti Malakar[1], Archana Singh[2] & Vinay Kumar Nandicoori[1*]

[1] National Institute of Immunology, Aruna Asaf Ali Marg, New Delhi, India.
[2] CSIR-Institute of Genomics and Integrative Biology, New Delhi, India.

Running Title: Deciphering the roles of RodA and PbpA in mycobacteria

Keywords: Transpeptidase, RodA, PbpA, cell division, LipidII, transglycosylase

* To whom correspondence may be addressed: Vinay Kumar Nandicoori, National Institute of Immunology, Aruna Asaf Ali Marg, New Delhi, India. Tel.: 91-11-26703789; Fax: 91-11-26742125; E.mail: vinaykn@nii.ac.in.

The cell wall of *Mycobacterium tuberculosis* (*Mtb*) is a complex structure that protects the pathogen in hostile environments. Peptidoglycan (PG), which helps determine the morphology of the cell envelope, undergoes substantial remodeling under stress. This meshwork of linear chains of sugars, crosslinked through attached peptides, is generated through the sequential action of enzymes termed transglycosylases and transpeptidases. The *Mtb* genome encodes two classical transglycosylases and four transpeptidases, the functions of which are not fully elucidated. Here, we present work on the yet uncharacterized transpeptidase PbpA and a non-classical transglycosylase RodA. We elucidate their roles in regulating *in vitro* growth and *in vivo* survival of pathogenic mycobacteria. We find that RodA and PbpA are required for regulating cell length, but do not affect mycobacterial growth. Biochemical analyses show PbpA to be a classical transpeptidase, while RodA is identified to be a member of an emerging class of non-canonical transglycosylases. Phosphorylation of RodA at T463 modulates its biological function. In a guinea pig infection model, RodA and PbpA are found to be required for both, bacterial survival as well as formation of granuloma structures, thus underscoring the importance of these proteins in mediating mycobacterial virulence in the host. Our results emphasize the fact that while redundant enzymes likely compensate for the absence of RodA or PbpA during *in vitro* growth, the two proteins play critical roles for the survival of the pathogen inside its host.

Mycobacterium tuberculosis (Mtb) cell wall is a complex structure that provides osmotic stability, drug resistance, enhanced virulence(1-3) and protects it from stress conditions in the host, such as reactive oxygen species (ROS), starvation, and hypoxia(4-9). Peptidoglycan (PG), a primary morphological determinant of the cell envelope, is a covalently linked network of glycan chains bridged through peptide bonds(10). PG synthesis is critically regulated to rheostat the cell growth and division for optimal bacterial survival. The initial steps of PG biosynthesis from UDP-GlcNAc to LipidII are performed in the bacterial cytoplasm by Mur family of enzymes (Fig 1). Subsequently, LipidII anchored to the intracellular membrane is flipped into the periplasmic space by flippase followed by transglycosylation, wherein the sugar moieties are linked to the existing chain through glycosidic bonds, via transglycosylases. Subsequent cross-linking of peptides through transpeptidation by **p**enicillin **b**inding **p**roteins (PBPs) completes the cross-linked protective PG structure (Fig 1). Due to the limited pool of available LipidII molecules(11,12), the enzymes involved in its synthesis, transport and utilization are excellent targets for therapeutic intervention(13-15). Recently,

Downloaded from http://www.jbc.org/ by guest on March 31, 2018

a new class of antibiotic, Teixobactin, a specific inhibitor of LipidII, has been shown to effectively kill multiple gram-positive bacilli including drug-resistant *Mtb*(16).

LipidII amounts are regulated in the periplasmic space through the enzymes involved in its flipping (LipidII flippase) and utilization (transglycosylase). The identity of LipidII flippases involved in regulating its levels in the periplasmic space varies among different classes of bacteria. FtsW in *Escherichia coli,* RodA in *Corynebacterium glutamicum,* MurJ from multiple bacterial species, Wzk from *Helicobacter pylori* and AmiJ from *Bacillus subtilis*(17,18) have been demonstrated to function as LipidII flippases(19-22). Presence of multiple candidates capable of performing LipidII flippase activity suggests functional redundancy and possible spatiotemporal regulation. MviN (a homolog of MurJ), FtsW and RodA are hypothesized to function as possible LipidII flippase in *Mtb*. Conditional depletion of MviN (an essential protein for *in vitro* growth) in *M. smegmatis* (*Msm*) leads to the accumulation of PG precursors in the cytosol, thus suggesting a possible role for MviN as a flippase(23). RodA, FtsW and SpoVE are members of the **s**hape, **e**longation, **d**ivision and **s**porulation (SEDS) family of proteins, with as yet ill-defined roles in cell wall biosynthesis during growth, division and sporulation(24). Interestingly, recent studies have uncovered a novel role for RodA as an unconventional transglycosylase in *B. subtilis* and *E. coli*(25-27). However, the role of FtsW or RodA remains uncharacterized in mycobacteria to date.

Mycobacterial genome encodes for ten PBPs, which can be broadly categorized into three classes based on their functions(28). Class I consists of two subclasses A and B; Class-A comprises of bifunctional enzymes that possess both transglycosylase and transpeptidase activities and Class-B enzymes are monofunctional with only the transpeptidase activity. In *Mtb*, there are four Class-I High Molecular Weight (HMW) PBPs, namely PonA1, PonA2, PbpA and Pbp3. Whereas PonA1 and PonA2 can perform both transglycosylase and transpeptidase activities, PbpA and Pbp3 can only carry out transpeptidation reaction. There are six enzymes belonging to Class II and III PBPs, which function as carboxypeptidases and β-lactamases involved in the maintenance of PG. With the exception of Pbp3, all the remaining PBPs are non-essential for *in vitro* growth. The genes encoding SEDS members are found in proximity with the genes of Class B PBPs, suggesting functional association among them (25). One such example is FtsW and Pbp3, which are shown to work as a pair in PG biosynthesis in *E. coli* and Mycobacterium species(26,29,30). RodA and PbpA, which are located next to each other, are also hypothesized to work as a pair, however, their roles in cell division and PG biosynthesis remain to be characterized.

Genes encoding for mycobacterial *rodA* and *pbpA* are located in the same operon that carries serine/threonine phosphatase *pstP* and two-serine/threonine protein kinases (STPKs) *pknA* and *pknB*(31) (Fig 2a). We have previously reported that PknA, PknB and PstP are independently essential for *in vitro* growth as well as *in vivo* survival of *Mtb*(32-34). Previous studies by multiple groups have suggested important roles for STPKs in regulating cell division and cell wall synthesis processes (35-37). Owing to the presence of *rodA* and *pbpA* in the *pknA* and *pknB* operon (Fig 2a), these genes are also speculated to play roles in modulating cell division and cell wall synthesis. The data presented in this study provide the first insight into the roles of *rodA* and *pbpA* genes in mycobacterial morphology, growth, and survival *in vitro* and *in vivo*.

RESULTS

Overexpression of RodA and PbpA leads to cell length elongation in Mtb.

To delineate the role of RodA and PbpA on mycobacterial cell morphology regulation, we sought to determine the impact of overexpression of these proteins in *Mtb*. Towards this, *rodA* and *pbpA* genes were cloned downstream of the tetracycline-inducible promoter in pST-KT vector(38) and the plasmids were electroporated into *Mtb*. Transformants were fixed six days post induction followed by scanning electron microscopy (SEM) analysis. A distinct increase in the cell length of the transformant bacteria was observed, with average cell length of *Mtb::rodA* and *Mtb::pbpA* in nutrient

Downloaded from http://www.jbc.org/ by guest on March 31, 2018

rich 7H9 medium increasing from ~1.9 μm to 2.34 μm and 2.18 μm, respectively (Fig 2b-c). The increase in the average cell length was more noteworthy in nutrient limiting Sauton's medium, wherein it increased from ~2.1 μm to ~2.8 μm in case of both transformant types (Fig 2 b-c). Similar results were obtained in *M. smegmatis* (*Msm*) transformants (Fig S1a-b). It is possible that the cell length elongation phenotype observed is due to their probable roles in PG biosynthesis. Overexpression may have resulted in uncoordinated PG biosynthesis, and consequently, increase in bacterial cell lengths.

RodA and PbpA play independent roles in modulating bacterial cell length.

While *E. coli rodA* and *pbpA* orthologs are essential genes, they are not essential in mycobacteria(39,40). To examine the functions of RodA and PbpA in modulating growth and morphology *in vitro* and survival *in vivo* (both, independently and combinatorially), *rodA, pbpA* and *rodA-pbpA* gene replacement mutant in *Mtb* and *Msm* strains were made using recombineering method(41)(Fig 3a & Fig S1c). PCR analysis with specific primer pairs confirmed the replacement of the genes with *hyg*^{r} marker at the native locus (Fig 3b & Fig S1d-e). Since *rodA* and *pbpA* are located upstream of essential kinases *pknA* and *pknB* and downstream of essential serine/threonine phosphatase, *pstP*, it is necessary to ascertain any polarity effects in the deletion mutants. Western blot analysis of lysates isolated from wild type and mutant strains showed comparable expression of PstP, PknA, PknB and GroEL-I (control), indicating that gene replacement mutants are devoid of any polarity effects both in *Mtb* (Fig 3c) and *Msm* (Fig S1f). We evaluated the impact of deleting *rodA* or *pbpA,* or both *rodA and pbpA,* on mycobacterial survival by enumerating CFUs on different days in growth kinetics for both 7H9 and Sauton's media. No significant differences were observed (Fig 3d-e), leading us to conclude that deletion of *rodA* or *pbpA* or both does not impact *in vitro* growth of *Mtb*. Unlike in *E. coli,* where conditional depletion of RodA or PbpA alters the cellular morphology from rod to round shape(42), no drastic changes in the morphology of mycobacterial deletion mutants was observed in our SEM studies (Fig 4a-b). However, while *MtbΔr* cells shortened significantly in both 7H9 and Sauton's medium, *MtbΔp* cells showed no significant difference in 7H9 medium but minor and significant changes in bacterial cell lengths in nutrient-limiting Sauton's medium (Fig 4c-d). More apparent defects in nutrient limiting Sauton's medium in comparison with rich 7H9 medium upon overexpression or deletion could be due to pertinent roles played by these proteins under stress conditions. To analyze if the cell length phenotype was dependent on growth phase we grew all the strains in Sauton's medium for different periods of time (0, 3, 6 and 9 days) before analyzing the cell lengths with the help of SEM. While the shorter cell length phenotype observed with *MtbΔr* was observed at every time point, the cell length phenotype altered across the growth phases in *MtbΔp* and *MtbΔrp* strains (Fig 4e). In case of *MtbΔp* and *MtbΔrp* the cells were initially shorter. However, at the later phase of growth (day 6 and 9) the cells were more elongated, consistent with observations in Fig 4d. These differences could be due to nutrient limitations as the growth progresses, leading to the necessity of higher levels of redundant enzymes such as PBPs involved in peptidoglycan synthesis. To confirm that the observed aberrations in the cell length were due to absence of RodA or PbpA, we performed complementation studies to rescue the mutant phenotypes by episomal expression of the respective proteins. The anomalous cell lengths observed in *MtbΔr* and *MtbΔp* cells were successfully reversed upon complementation (Fig 4f).

Wild type and gene replacement mutant strains of *Mtb* were subjected to TEM analysis to evaluate the impact of gene deletions on cell wall ultrastructure (Fig 5a-d). While the wild type and deletion mutants grown in 7H9 medium showed no significant difference in cell wall ultrastructure (Fig 5a & 5c), we observed conspicuous changes in the cell wall architecture of *MtbΔp* and *MtbΔrp* in

Downloaded from http://www.jbc.org/ by guest on March 31, 2018

Sauton's medium as compared with the *Mtb* and *MtbΔr* strains (Fig 5b and 5d). The outermost electron-dense opaque layer of *MtbΔp* and *MtbΔrp* was strikingly thicker (~30 nm) as compared with *Mtb* (~18nm) and *MtbΔr* (~15.9nm). We speculate that the observed phenotype for *MtbΔp* and *MtbΔrp* mutants could be an adaptive response to the compromised cellular fitness under nutrient limiting conditions. Thus, we evaluated the possible impact of deletion of *rodA* or *pbpA* on survival under hypoxia and persistence (Fig 5e-f). In line with the results above, we observed decreased survival only with the *MtbΔp* mutant in Wayne model of hypoxia(43) (Fig 5e). However, in persisters analysis wherein *Msm* wild type and mutant cultures were exposed to 10 μg/ml of isoniazid, both *MsmΔr* and *MsmΔp* mutants showed 10-fold decline in CFUs (Fig 5f). Taken together these data suggest that both RodA and PbpA may play a role in combating survival under different stress conditions.

PbpA functions as a transpeptidase

RodA and PbpA function at different stages of PG biosynthesis (outlined in Fig 1). RodA has been shown to function either as a LipidII flippase in *E. coli* and *C. glutamicum,* or more recently, as a non-canonical transglycosylase in *B. subtilis*(25). Based on sequence homology and crystal structure, PbpA is annotated as a transpeptidase(44). To identify the stages of the PG biosynthesis pathway at which mycobacterial RodA and PbpA function, we began with determining the (viability) sensitivity of *Msm, MsmΔr* and *MsmΔp* strains to various inhibitors known to act at different steps of the PG biosynthesis pathway (Fig 1). As expected, *Msm, MsmΔr* and *MsmΔp* strains showed similar sensitivity to isoniazid - an inhibitor of InhA, an enzyme involved in mycolic acid synthesis. However, *MsmΔp* showed much higher sensitivity to oxacillin+clavulanic acid (oxacillin: a pan-inhibitor of transpeptidases; clavulanic acid: a potent inhibitor of β-lactamases which enhances the inhibitory potential of oxacillin) compared to *MsmΔr* or *Msm* (Fig 6a), which is consistent with its predicted role as a transpeptidase. *In-trans* complementation of PbpA restored the sensitivity values closer to *Msm* (Fig 6b).

To evaluate PbpA transpeptidase activity Bocillin-FL labeling assays were performed as described earlier (45). Bocillin-FL is essentially pencillin tagged with a flourescent probe, which forms a stable covalent intermediate with the catalytically active transpeptidase enzymes. Membrane fractions prepared from *Msm*, *MsmΔp, MsmΔp* complemented strains were incubated with Bocillin-FL, reactions resolved by gel electrophoresis, and the gels analyzed by scanning them. Although we could detect a band of the appropriate molecular weight corresponding to PbpA (~50 kDa) in case of the *Msm* membrane fraction, the same was absent in *MsmΔp* membrane fraction, suggesting that PbpA is indeed a transpeptidase (Fig 6c). Structural analysis of $PbpA_{Mtb}$ suggested S281 and K424 residues to be a part of the catalytic site (44). We generated PbpA-S281A and PbpA-K424G mutants and investigated their ability to rescue the depleted transpeptidase activity of *MsmΔp*. While wild type and PbpA-S281A mutants could rescue the lost transpeptidase activity (Fig 6c; shown by arrows), PbpA-K424G complementation did not, suggesting that the K424 residue plays an important role in mediating the transpeptidase activity of PbpA.

RodA functions as a non-canonical transglycosylase

Next, we evaluated the role of RodA by assessing the sensitivity of *rodA* deletion mutant towards nisin and vancomycin. Nisin is an inhibitor, which binds to the pyrophosphate group of LipidII, forms pores in the membrane and eventually leads to cell death. If RodA were to function as a LipidII flippase, the absence of RodA would result in reduced levels of LipidII in the periplasmic space. In *C. glutamicum* where RodA functions as a LipidII flippase, deletion of *rodA* resulted in resistance towards nisin(20). Previous data has established that enhanced LipidII content leads to higher sensitivity to nisin(46). We observed that RodA deletion (but not deletion of PbpA) resulted in higher sensitivity of *Msm* towards nisin (Fig 6a and Table 1). Vancomycin is another sensor of LipidII, which binds to the D-Ala-D-Ala terminal amino acids of the pentapeptide in LipidII, inhibiting nascent PG biosynthesis(13). Approximately 8-fold higher

Downloaded from http://www.jbc.org/ by guest on March 31, 2018

sensitivity of *MsmΔr* to vancomycin compared with *Msm* was noted, thus clearly omitting the possibility of RodA functioning as a flippase in mycobacteria (Fig 6a and Table 1). The enhanced sensitivity of *MsmΔr* to nisin and vancomycin suggests the possibility of higher accumulation of LipidII molecules in the periplasmic space of *MsmΔr* mutant, which could be due to hampered non-canonical transglycosylase activity of RodA. To investigate if higher levels of LipidII molecules are accumulated in *MsmΔr* cells compared with wild type *Msm* cells we pulsed actively growing *Msm* and *MsmΔr* cultures with ^{3}H-mesoDAP (^{3}H-mDAP) for ~4-5 h to label the lipid- linked peptidoglycan precursors including LipidII (Fig 6d). Equal quantities of these cells were processed for small-scale LipidII accumulation analysis(47) and the amount of ^{3}H-LipidII was quantitated. We observed a consistent ~20% increase in the counts, suggesting that the increased sensitivity to Nisin and Vancomycin is indeed due to higher accumulation of LipidII.

The possibility of RodA functioning as a non-canonical transglycosylase was evaluated by investigating the sensitivity of wild type and mutants to moenomycin. Moenomycin specifically targets the active site of canonical PG glycosyltransferases (transglycosylases), leading to compromised cell wall, resulting in cell content leakage and eventual death(48). If mycobacterial RodA were to function as a non-canonical transglycosylase, the *MsmΔr* deletion mutant would exhibit hypersensitivity to moenomycin compared with *Msm*. In line with this hypothesis, *MsmΔr* strain was ~6 fold more sensitive compared with *Msm* (Fig 6e and Table1a). Notably, while *in-trans* expression of both *Msm* and *Mtb* RodA efficiently restored the moenomycin sensitivity defect, *in-trans* expression of FtsW or MviN failed do so (Fig 6e and Table 1b). Streaking *Msm, MsmΔr* and complemented strains on the plates in the presence or absence of 1 μg/ml moenomycin substantiated the above data (Fig 6f). Based on these data we suggest mycobacterial RodA to be part of an emerging class of non-canonical transglycosylases.

Amino acid residues critical for transglycosylase function are conserved in mycobacterial RodA.

RodA is a well-conserved protein across the bacterial species. Random mutagenesis of *B. subtilis* RodA has identified a number of residues that are indisputably critical for its function(25). On analysis of the primary sequence of mycobacterial RodA we found ~80% of these residues to be conserved (data not shown). The amino acid residues D105 and W280 present in the periplasmic loop region of *B. subtilis* RodA have been biochemically demonstrated to mediate transglycosylase activity in *B. subtilis*(25). These residues were found to be positionally conserved in the putative periplasmic loop regions of *Mtb* and *Msm* RodA at D343/344 and W175/176, respectively (Fig 7a). In order to determine the roles of these conserved D and W residues in mycobacteria, we generated *Msm rodA* deletion strains complemented with point mutants of these residues in *Mtb* and *Msm* RodA. Similar to our previous observations (Fig 6e), we found *MsmΔr* mutant to be ~4-6-fold sensitive to moenomycin compared with *Msm*. However, while *in-trans* expression of wild-type RodA from *Mtb* or *Msm* could rescue the sensitivity phenotype, expression of either single or combinatorial mutant of D and W residues of RodA failed to complement this moenomycin sensitivity defect. Growth of *MsmΔr* and *MsmΔr* complemented with D and W point mutants from both *Mtb* and *Msm rodA* was also specifically attenuated in presence of moenomycin on solid media on plates (Fig 7b-c). In addition, MIC analysis of these mutants in liquid media also yielded similar defect profiles (Fig 7d and Table 1b). Thus, collectively we can say that conserved catalytic residues D343/344 And W175/176 are critical for the non-canonical transglycosylase activity of mycobacterial RodA.

RodA is phosphorylated on T463 residue.

In mycobacteria, phosphorylation of proteins are shown to regulate multiple processes including mycolic acid synthesis, peptidoglycan synthesis, cell division and cellular localization(32,49,50). PG biosynthesis is a spatiotemporally coordinated event requiring synchronized interactions between numerous proteins involved in cell division and cell wall

Downloaded from http://www.jbc.org/ by guest on March 31, 2018

synthesis. High-throughput analysis of phosphoenriched lysates from *Mtb* led to the reproducible identification (two of three biological replicates) of a phosphorylation event at T463, a residue belonging to the carboxy terminal cytosolic tail region of RodA (Fig 8a). We sought to identify the serine/threonine protein kinases (STPKs) involved in mediating the phosphorylation of T463 residue of RodA. We were unable to express and purify full-length recombinant RodA due to its poor expression and solubility, perhaps due to the presence of twelve transmembrane domains in the protein (51,52). Hence, we cloned and purified the carboxy terminal $RodA_{441-469}$ fragment with N-terminal His tag (Fig 8b; right panel). We next purified ten MBP-tagged STPKs from a system we have developed previously(49) (Fig 8b). *In vitro* kinase assays performed with purified STPKs showed that both PknB and PknH robustly phosphorylate $RodA_{441-469}$ (Fig 8c). In addition to the above kinases PknG, PknD and to an extent PknL also mediate $RodA_{441-469}$ phosphorylation (Fig 8c). Together, the data suggests that PknB and PknH are the likely kinases involved in phosphorylating RodA *in vivo*.

To investigate the functional significance of phosphorylation at T463 residue of RodA we mutated the T463 residue to phosphoablative (T463A) or phosphomimetic (T463E) residues. Towards assessing the role of phosphorylation in modulating catalytic activity of RodA, we evaluated the sensitivity of *MsmΔr* cells to moenomycin when complemented with wild type as well as phosphoablative and phosphomimetic mutants. Both wild type and phospho mutants rescued the moenomycin sensitivity phenotype (data not shown), suggesting that phosphorylation does not play any role in modulating non-canonical transglycosylase activity of RodA. Next, we analyzed the impact of phosphorylation on restoring cell length defects observed in the mutant. SEM analysis of *Mtb*, *MtbΔr* and *MtbΔr*::*r* complemented strains was consistent with the results in Fig 4, wherein we observed decrease in the cell length upon deletion of *rodA* that was rescued by episomal expression of RodA. The aberrant short length phenotype could be rescued upon *in-trans* expression $RodA_{T463E}$, however, the phosphoablative mutant $RodA_{T463A}$ failed to rescue the phenotype, suggesting that phosphorylation of T463 residue is important for the function of RodA (Fig 8d-e). The C-terminus of *Corynebacterium glutamicum* RodA modulates its interaction with DivIVA (homolog of $Wag31_{Mtb}$). We speculate that phosphorylation may play an important role in modulating such interactions, thus explaining the inability of phosphomimetic mutant to rescue the observed cell length defective phenotypes.

RodA and PbpA mutants show compromised bacterial virulence in the host

To investigate the roles of RodA and PbpA in the ability of *Mtb* to establish infection and survive in the host, we initiated studies using the mouse infection model. We challenged Balb/c mice aerosolically with *Mtb*, *MtbΔr, MtbΔp* and *MtbΔrp* strains, and colony-forming units (CFUs) were enumerated one-day post infection to determine the initial bacillary deposition. This was found to be similar in case of all the strains (Fig 9a). Disease progression as assessed by the gross evaluation of lungs and spleen (data not shown) and lung bacillary load four weeks post-infection revealed marginal differences between infection by *Mtb* versus the mutant strains, suggesting that absence of *rodA* and *pbpA* had no impact on mycobacterial survival in the mice model as host (Fig 9a). We have taken the mice infection experiment to 12 weeks (data not shown) and have not found any significant differences in the bacterial survival between wild type and mutant strains.

Since granulomas, the hallmark of human pulmonary tuberculosis, are absent in the mouse infection model(53), we used the guinea pig model to study this aspect(54). Accordingly, guinea pigs were infected aerosolically to evaluate the roles of RodA and PbpA in maintenance of recalcitrant non-replicating bacilli in such structures. While the lungs of guinea pigs infected with *Mtb* showed presence of discrete tubercles, we observed reduction in such tubercles in the lungs of *Mtb*Δ*r* and *Mtb*Δ*p* infected guinea pigs (Fig 9b; shown with white arrows). Bacillary survival in lungs evaluated four weeks post-infection revealed the attenuated survival of *MtbΔr,*

Downloaded from http://www.jbc.org/ by guest on March 31, 2018

MtbΔp and *MtbΔrp,* exhibiting 2, 10 and 5-fold lower bacillary load respectively as compared with *Mtb* (Fig 9c). However, the splenic loads for wild-type and the mutant strains were found to be similar (Fig 9d). Interestingly, histopathological analysis revealed that irrespective of the bacillary load in lungs or spleen, the granuloma scores were consistently lower in case of all the mutants both in lungs and spleen when compared with the wild type (Fig 10). The lower granuloma scores are indicative of a compromised niche that would affect long-term survival. Thus, based on compromised survival studies and lower histopathological scores, obtained in case of all the deletion mutants (Fig 10), we suggest that RodA and PbpA play crucial roles in imparting mycobacterial virulence in the host.

DISCUSSION

The mycobacterial cell wall is the primary barrier protecting the cell from host-mediated stress and undergoes substantial remodeling in the host(55). Maintenance of cell integrity and shape requires the coordinated regulation of cell wall biosynthesis and cell division processes. Bacterial cell growth broadly has two distinct stages: elongation, and subsequent division of the cell. Synthesis of PG - an integral part of the cell wall - takes place at both- poles and septum and is critically regulated to sustain optimal bacillary growth and survival. The cellular machinery associated with PG biosynthesis at poles and septum are termed as elongasome and divisome respectively(56). These complexes are thought to function independently, yet in a coordinated manner to preserve the integrity of cell growth and division processes. SEDS and PBP family of proteins function in pairs and modulate PG biosynthesis within these elongasome and divisome complexes - for example, based on interaction and localization studies, FtsW-Pbp3 pair from *E. coli* and mycobacteria is shown to function in the divisome(26,29,30). In most cases, SEDS-PBP pairs are genetically linked and exhibit high phylogenetic conservation. *RodA* and *pbpA,* located next to each other in the same operon (Fig 2), are members of SEDS and PBP family respectively and are thus speculated to be functionally correlated(25). In *S. pneumoniae*(57) *and E. coli*, RodA directly interacts with Pbp2B (homolog of *Mtb* PbpA)(58) and in *C. glutamicum* with DivIVA (homolog of *Mtb* wag31)(59), a known determinant of apical/polar growth, and these interactions are critical for appropriate localization of elongasome. The present study aimed to examine the functions of mycobacterial RodA and PbpA by overexpressing and generating gene replacement mutants and analyzing their phenotypes obtained *in vitro* and *in vivo* (Fig 2-3).

If RodA and PbpA were to function as a pair, one would expect that the cellular morphology would be similar when either of them is overexpressed or deleted. While the overexpression of either RodA or PbpA resulted in similar phenotype of elongated cells, deletion of either of them gave contrasting phenotypes (Fig 2-4). Whereas the cells were elongated upon *pbpA* deletion, we observed the cells to be shorter upon *rodA* deletion (Fig 4). PbpA is known to interact with FhaA, an FHA domain containing protein and localize to both poles and septum(60). While mycobacterial PbpA protein interacts with CrgA, a probable scaffold recruiter protein at the divisome, RodA fails to do so. Thus, we hypothesize that RodA and PbpA are most likely participating in different complexes(61). We observed significant changes in the cell wall architecture upon PbpA deletion (both in single and combinatorial mutant) in limiting medium conditions (Fig 5). Such thickened cell wall architecture is typically observed in micro-aerobically or anaerobically grown *Mtb,* and is believed to serve the purpose of protecting the bacteria in hypoxic conditions(62). Based on the above findings and the phenotypes observed, we suggest that PbpA and RodA may function in different complexes, with PbpA playing an important role in stress adaptation.

PbpA is predicted to be a transpeptidase involved in cross-linking of stem peptides attached to NAM in the PG monolayer(44). In line with this prediction, absence of *pbpA* resulted in higher susceptibility to β-lactam antibiotics (Fig 6). Furthermore, biochemical assays revealed PbpA to be classical transpeptidase with a role for K424 in the catalysis (Fig 6). Unlike in mycobacteria, *rodA* is

Downloaded from http://www.jbc.org/ by guest on March 31, 2018

indispensable in a number of other bacteria and its conditional depletion results in conversion of bacterial rods to spheres(20,42,63,64). Based on sequence and structural conservation with FtsW, RodA has been proposed to function as lipid II flippase(24,65). In contrast, recent studies performed in *B. subtilis* suggested a novel role for RodA as a non-canonical transglycosylase, which upon overexpression can compensate for the absence of all classical PBPs with transglycosylase function(66). If mycobacterial RodA were to function as a LipidII flippase, one would expect lower levels of LipidII in periplasmic space upon its deletion(20). On the other hand, if RodA were to function as a transglycosylase, its absence would result in accumulation of LipidII in the periplasmic region. We observed increased sensitivity of mycobacterial *rodA* deletion mutant to vancomycin and nisin (Fig 6), indicative of LipidII accumulation(46) in the periplasmic space, strongly suggesting that RodA is likely to function as a transglycosylase rather than a LipidII flippase. In addition, small-scale LipidII accumulation analysis performed with ^{3}H-mDAP (an exclusive component of PG precursor) also suggested ~20% higher accumulation of LipidII (Fig 6). *B. subtilis* conditional *rodA* mutant is hypersensitive to moenomycin, an inhibitor of canonical transglycosylases(27). In line with this, we found mycobacterial *rodA* mutant to be hypersensitive to moenomycin (Fig 6). Importantly, while *in trans* expression of *Msm* and *Mtb rodA* could rescue moenomycin sensitivity defects, expression of *ftsW* or *mviN* failed do so. Meeske et al. have identified immutable residues in *B. subtilis* RodA that are necessary for its function(25). Furthermore, biochemical experiments revealed a definitive role for W_{105} and D_{280} residues in modulating transglycosylase activity(25). In agreement with this, *in trans* expression of mycobacterial RodA point mutants, wherein residues corresponding to conserved W and D have been mutated, failed to rescue the moenomycin sensitivity defect of *rodA* deletion mutant (Fig 7). Taken together, this is the first data demonstrating RodA function as a non-canonical transglycosylase in mycobacteria.

Phosphorylation events have been shown to regulate various cellular processes, including cell wall biosynthesis and cell division (36,37). STPKs PknA and PknB have been shown to phosphorylate many target proteins including those involved in PG biosynthesis such as Wag31, FtsZ, MviN, MurD and GlmU(23,50,67-69). Phosphorylation of these proteins has been implicated in modulating their enzymatic activities, cellular localization, or protein-protein interactions(50,67,70). Mass spectrometry analysis of phosphoenriched *Mtb* lysates identified phosphorylation at T463 of *Mtb* RodA (Fig 8). Our results are in agreement with an independent study, wherein RodA was identified to be phosphorylated at T463 in *M. bovis* BCG(71). *In vitro* kinase assays with purified STPKs showed that PknB and PknH are the most likely STPKs to mediate phosphorylation of RodA (Fig 8). Interestingly, while *in trans* complementation of *MtbΔr* with phosphoablative mutant failed to rescue the short length phenotype, complementation with phosphomimetic mutant fully complemented the mutant phenotype (Fig 8). While RodA is a structurally conserved protein, so far, no post-translational modifications (and their role in modulating RodA activity) have been identified in other bacterial systems. Interestingly, in *C. glutamicum,* the negative charges on the carboxy-terminal residues of RodA have been shown to a play a role in modulating interactions with DivIVA (homolog of Wag31)(59). We speculate that the phosphorylation of RodA in the carboxy-terminal region, specifically at T463, may be important for modulating its interactions with other cell division proteins, thus regulating the cell division process.

Bacterial shape and its evolution have been related to better survival in diverse milieus(72). Bacterial cell shape and dimensions are determined by the cell wall and its composition. The composition of the *Mtb* cell wall undergoes changes to adapt to and impart drug tolerance under stress conditions, and its remodeling events are critical for infection in macrophages(73). The composition of the bacterial cell wall is an important factor in modulating fitness by regulating adherence to biotic surfaces, efficient survival under nutrient-deprived and stress conditions, efficient nutrient uptake and passive dispersal(74). Enzymes involved in PG biosynthesis have been shown to play an important role in maintaining cell shape and survival under

Downloaded from http://www.jbc.org/ by guest on March 31, 2018

stress(75). The deletion of enzyme decaprenol pyrophosphatase (UppP) involved in PG precursor LipidII synthesis results in severe attenuation in mice model of infection(76). Deletion of *ponA1,* a PBP protein with transglycosylase and transpeptidase activities, displayed compromised survival in mice(70).

RodA and PbpA are involved at different steps of peptidoglycan synthesis. In *Streptococcus thermophilus,* RodA and PbpA play a role in combating oxidative stress(77-79). Mycobacterial PbpA has been found to be upregulated under nutrient starvation conditions mediated via stringent response regulator RelA, which is required for the long-term survival of pathogen in mice and guinea pigs(80,81). Moreover, expression of both *Mtb rodA* and *pbpA* is upregulated under SDS and diamide stress, possibly due to their role in stress adaptation. The observed differences in the cell length phenotypes observed upon overexpression and deletion of RodA and PbpA are not very large but are observed consistently (Fig 2 and 3). Thus, we speculated that either *rodA* or *pbpA* or both might play a role in survival of pathogen in the host.

Interestingly, we did not observe any significant difference between wild-type and mutant strains in the bacillary loads in mice infection experiments at any time point post-infection (Fig 9). Since hypoxic granulomas with necrotic lesions are not detected in the lungs of infected mice, they are viewed as inappropriate models for investigating paucibacillary state observed in the human infections(53,82). On the other hand, guinea pigs harbor the hallmark hypoxic granuloma structures that mimic the diseased state in humans(54). Importantly, in our guinea pig model infection studies, we observed ~ 0.5 to 1 log fold (5 to 10-fold) decrease in the survival of pathogen in the lungs of guinea pigs infected with *MtbΔr* or *MtbΔrp or MtbΔrp* mutants (Fig 9). Moreover, the corresponding granuloma scores for mutants were almost 50% lower compared with the wild type (Fig 10). In case of spleen, while the infection loads were similar, the granuloma scores mirrored the compromised scores for lungs. The granuloma architecture in *Mtb*-infected guinea pig is highly organized, hypoxic with necrotic lesions, and harbor recalcitrant non-replicating bacilli, close to diseased state in humans(54). Thus, we suggest that rodA and pbpA play a role in long term mycobacterial survival in the host. Further experiments in guinea pig model with protracted time points would be required to conclusively demonstrate their roles in long term survival.

We also observed decreased survival of *pbpA* mutant in *in vitro* Wayne model of hypoxia(43) (Fig 5e). Persisters analysis for deletion mutants of *rodA* and *pbpA* exhibited 10-fold decline in CFU upon exposure to 10 μg/ml of isoniazid (Fig 5f). The data collectively underscore the importance of RodA and PbpA in mediating survival under hypoxic conditions *in vivo*. In line with this thinking, muramyl dipeptides which are a part of PG have previously been shown to activate macrophages, and when associated with branched fatty acids, they promote granuloma formation(83). Taken together, using the guinea pig infection model we report here for the first time a role for PG biosynthetic proteins RodA and PbpA in modulating survival of the human pathogen *Mtb* in the host.

EXPERIMENTAL PROCEDURES

Bacterial Strains and reagents

Constructs and strains used in this study are listed in Table-2. Oligonucleotides and fine chemicals were purchased from Sigma, Amresco, Merck and Bio Basic. Restriction and modification enzymes were purchased from New England Biolabs (NEB) or MBI-Fermentas (Thermo Scientific). pENTR/Directional TOPO Cloning Kit and BOCILLIN™ FL Penicillin, Sodium Salt was purchased from Invitrogen and growth medium from BD Difco. pMAL-c2x(NEB) kinase clones constructs already available in lab were used for purification(49). ^{3}H-meso-diaminopimelic acid (^{3}H-mDAP) was purchased from American Radiolabelled Chemicals (ARC) and γ[^{32}P]ATP was purchased from PerkinElmer Life Sciences. pNiT-I vector was a kind gift from Prof. Christopher M. Sassetti(84). pNit-ET was a kind gift from Prof. Eric Rubin(85). α-FLAG monoclonal antibody was purchased from Sigma. α-PknB, α-PknA and α-GroEL-I antibodies were generated in the lab and α-

Downloaded from http://www.jbc.org/ by guest on March 31, 2018

PstP antibody was a kind gift of Dr. Yogendra Singh, IGIB(86). Electron microscopy chemicals were purchased from Electron Microscopy Sciences.

Generation of plasmid constructs

pNit-Cm was generated by inserting blunt-ended chloramphenicol resistance gene (*cm*^{r}) from pENTR-Cm^r, into PflMI-linearized and filled-in pNit vector. *RodA*, *pbpA, ftsW and mviN* genes were amplified using H37Rv genomic DNA as the template and the amplicons obtained were cloned into pENTR vector. The pENTR clones of *rodA* and *pbpA* were digested with NdeI and HindIII enzymes to release the *rodA* and *pbpA* genes which were then subcloned into the corresponding sites in pST-KT(38) and/or pNit-Cm vectors. $rodA_{411\text{-}469}$ as amplified using specific forward primer containing NdeI site and 3X Flag tag and gene specific reverse primer. 3X-$rodA_{411\text{-}469}$ amplicon was digested with NdeI HindIII was cloned into pET28b vector. Point mutants of *Mtb* and *Msm*-RodA-$rodA_{W175R/W176R}$, $rodA_{D343R/D344R}$ and $rodA_{W175R\text{-}D343R/W176R\text{-}D344R}$ were generated using *Mtb* or *Msm* genomic DNA with the help of overlapping PCR. Point mutants of *Mtb* PbpA- $pbpA_{S281A}$ and $pbpA_{K424G}$ were generated using *Mtb* genomic DNA with the help of overlapping PCR

Generation of gene replacement mutant construct

Gene replacement mutants of *rodA*, *pbpA* and *rodA-pbpA* together were generated in both *M. tuberculosis* H37Rv and *M. smegmatis* mc^{2}155 with the help of recombineering(41). Towards the generation of allelic exchange (AES) substrates, upstream (flank 1) and downstream flanks (flank 2) were amplified using genomic DNA as the template, apramycin resistance gene (*am*^{r}) was amplified from pMV261-apra(87), hygromycin res gene (*hyg*^{r}) and oriE+λ cos fragments were amplified from pYUB1471(88). Amplicons obtained were digested with PflMI/BstAPI and ligated in a five-piece ligation reaction. *M. smegmatis* and *M. tuberculosis* were electroporated with pJV53 and pNit-ET constructs to generate *Msm::JV53* and *Mtb::ET* strains. AESs were digested with restriction enzymes SnaBI or EcoRV to generate linear blunt-ended recombineering proficient (containing flank1-*hyg*^{r}-flank2) DNA fragments that were electroporated into recombineering proficient *Msm::JV53* and *Mtb::ET* strains. The recombinant deletion strains were confirmed by performing PCRs across the deletion junctions and the positive strains were cured of recombineering plasmids pJV53 and pNit-ET.

Growth analysis

Mtb (wt), rodA deletion mutant *(MtbΔr), pbpA* deletion mutant *(MtbΔp)* and *rodA-pbpA* double deletion mutant *(MtbΔrp),* were grown in Middlebrook 7H9 medium containing 10% ADC (albumin, dextrose and catalase) in presence or absence of 100 μg/ml hygromycin. Cultures were grown till absorbance (A_{600}) reached ~0.8 and the cells were harvested and washed with PBS containing 0.05% Tween-80 ($PBST_{80}$). For growth analyses, cultures were initiated at A_{600} ~0.1 in 7H9/Sauton's medium without antibiotics and incubated at 37ºC with shaking (100 rpm). A_{600} was measured every 24 hours for 6-10 days and serial dilutions of cultures were plated on 7H11 agar. CFUs were enumerated. Experiments were performed in triplicates and obtained average CFUs were plotted as a function of time. Standard errors were calculated using GraphPad Prism 6 for each time point.

Scanning Electron Microscopy (SEM) and Transmission Electron Microscopy (TEM)

Cells grown either in 7H9 or Sauton's medium were diluted to A_{600}~0.5. 10 ml of the cultures were harvested, and SEM and TEM were performed as described previously(69). For the quantification of cell length, ~200 individual cells were measured from the acquired SEM images using Smart Tiff software. The mean cell length and statistical significance (ANOVA test) were determined using GraphPad Prism 6 software.

Hypoxia experiments

Mtb, *MtbΔr* and *MtbΔp* cells were subjected to hypoxic conditions as described earlier (69). Bacterial survival was assessed at indicated time points by CFU enumeration. Persisters analyses of

Downloaded from http://www.jbc.org/ by guest on March 31, 2018

Msm, *MsmΔr* and *MsmΔp* strains were performed as described previously (89).

MIC determination

MIC determination was performed as described earlier with the help of Resazurin microtiter assay (REMA)(90). Briefly, different dilutions of antibiotics in Dubos medium with appropriate controls were added to a flat-bottomed 96-well plate. Cells grown in Dubos medium till early or late exponential phase were diluted to A_{600} of 0.006 in the same medium and 100 µl of each was added to each well of the 96-well plate containing different dilutions of antibiotics. The plates were incubated at 37°C for 24 h, and 20 µl of Resazurin solution (0.02%) was added to each well followed by overnight incubation at 37°C. Color transition from blue to pink was an indicator of bacterial growth. MIC was defined as lowest concentration of antibiotic that prevented this change in color.

Bocillin FL labeling assay

Cultures of *Msm, MsmΔp, MsmΔp::p MsmΔp::*p_{S281A} and *MsmΔp::*p_{K424G} strains were induced with 5µM IVN and the membrane fractions were prepared as described previously(91). Protein concentrations were estimated using Biorad Bradford Assay. For each strain, ~20 µg of transmembrane preparations in a 24 µl reaction volume was incubated with Bocillin FL (Invitrogen, Carlsbad, CA) in PBS for 20 min at 37°C in dark. Reactions were stopped by the addition of SDS-sample buffer followed by boiling for 5 min followed and incubation on ice for 5 min(92). Samples were resolved on 8% SDS-PAGE, gel was washed with MQ water for one h and fluorescence of the Bocillin-labeled proteins was detected using Typhoon Scanner (GE Healthcare) under 488 nm excitation and 532 nm emission conditions. Similar amount of membrane extracts were processed for immunoblot analysis.

RodA LipidII accumulation assay

Msm and *MsmΔr strains* were grown in Sauton's media till A_{600}~0.2-0.3 and pulsed with 1.5 µCi/ml ^{3}H-mDAP) (procured from ARC) for 4-5 h. Equal amounts of cultures were processed for small-scale LipidII accumulation analysis as described (47). Obtained Lipid fractions were dried using speed vac followed by the addition of scintillation fluid (Betaplate Scint Perkin Elmer) and overnight incubation. Radiolabeled ^{3}H-LipidII in the samples was quantified by scintillation counting using a β counter. Reading obtained for *Msm* in each independent experiment was normalized to 100% and the counts obtained for *MsmΔr* were represented as percent change with respect to counts obtained for *Msm*.

Identification of phosphorylation site

Mtb H37Rv strain was grown in 7H9-ADC medium till A_{600} ~0.8-1.0. Whole cell lysates (WCLs) were prepared in lysis buffer containing 8M urea in the presence of protease and phosphatase inhibitors. Trypsinization and **s**trong **c**ation e**x**change (SCX) chromatography of 10 mg of WCLs was performed as described previously(93). SCX fractions were phosphoenriched using TiO_2 beads and eluted in 0.3 M ammonium hydroxide followed by desalting. Fractions were resuspended in 20 µl solution containing 5% ACN and 0.1% formic acid. LC-MS analysis using LTQ Orbitrap Velos was performed as described earlier(94) and the data was analyzed using Proteome Discoverer Software Suite (version 1.3). For the search using SEQUEST, carbamidomethylation on cysteine residues was used as fixed modification, and oxidation of methionine and phosphorylation of serine, threonine, and tyrosine were used as variable modifications. Spectra were queried against the *Mtb* UniProt database.

***In vitro* kinase Assay**

pMAL-c2X constructs expressing *Mtb* STPKs generated by us previously(49) and pET-RodA $_{441-469}$ construct were transformed into *E. coli* BL21 (DE3) Codon Plus cells followed by expression and purification as described previously (49). *In vitro* kinase assay was performed as described earlier using ~10 pmoles of purified STPKs and 2 µg purified RodA $_{441-469}$ as substrate (95).

Mycobacterial infection of mice and guinea pigs

Mtb, MtbΔr, MtbΔp and *MtbΔrp* strains were grown in 7H9-ADC broth at 37°C, 100 rpm till A_{600}~0.6. Cells were harvested at 3000 g at RT and cell pellets

Downloaded from http://www.jbc.org/ by guest on March 31, 2018

were washed twice with sterile $PBST_{80}$ before resuspension in neutral buffered saline. Balb/c mice of either sex (six to eight weeks old) were obtained from the animal breeding facility at National Institute of Immunology. Mice (n=6) were infected with 2 x 10^8 CFUs by aerosol route. Bacillary loads in lungs were enumerated after day one and after 1, 2, 4 and 8 weeks post-infection(33). For infecting guinea pigs, outbred female guinea pigs of the Duncan-Hartley strain (weight 200-300 g) were infected with 10^8 CFUs through aerosol route to implant 100 CFU/lung. Bacillary loads in lung and spleen were enumerated 4 weeks post infection(69). Infected lungs and spleens were fixed in neutral buffered saline followed by hematoxylin and eosin staining. Histopathological evaluation and granuloma grading was performed as described in earlier study(69). Total granuloma score was obtained by adding the individual score for each type of granuloma.

Downloaded from http://www.jbc.org/ by guest on March 31, 2018

Acknowledgements.

We thank the Tuberculosis Aerosol Challenge Facility (DBT-TACF) staff Dr. Lakshyaveer Singh, Sudesh Rathour and Mahendra Singh at International Centre for Genetic Engineering and Biotechnology (New Delhi, India) for their kind help. We thank Dr. Dhiraj Kumar for extending the use of the TACF facility. We thank Suresh Kumar for his help in purification of MBP tagged STPKs. We thank TEM facility at CSIR-Institute of Genomics and integrative Biology, scanning electron microscopy facility and the biocontainment facility (BSL3) at the National Institute of Immunology. We thank Rekha Rani and Bhanu Mantri for their support in SEM/TEM. We thank Dr. Christopher Sassetti, Dr. Graham Hatfull, Dr. Eric Rubin, and Dr. William Jacobs for providing the constructs used in this study. We thank Dr. Swati Saha for critical reading of the manuscript.

Conflict of interest statement

The authors certify that they have no conflicts of interest in the subject matter of this article.

Funding Sources:

This work was supported by the funding provided by SERB, Department of Science and Technology, Government of India project EMR/2014/000877 to V.K.N. A.S. is supported by INSPIRE Faculty grant from Department of Science and Technology, Government of India.

Author Contributions

D.A., V.K.N. conceived and designed the experiments. D.A. performed most of the experiments, Y.C. performed Guinea pigs infection experiment; B.M. performed mass spectrometry studies and A.S. performed TEM studies. D.A. & V.K.N. analyzed the data and wrote the paper. All authors read and approved the manuscript.

Ethical Statement

Experimental protocol for the animal experiments was approved by the Animal Ethics Committee of National Institute of Immunology, New Delhi, India (the approval number is IAEC# 389/15). The approval is as per the guidelines issued by Committee for the Purpose of Control and Supervision of Experiments on Animals (CPCSEA), Govt. of India.

Downloaded from http://www.jbc.org/ by guest on March 31, 2018

REFERENCES

1. Barry, C. E., Crick, D. C., and McNeil, M. R. (2007) Targeting the formation of the cell wall core of M. tuberculosis. *Infect Disord Drug Targets* **7**, 182-202
2. Kaur, D., Guerin, M. E., Skovierova, H., Brennan, P. J., and Jackson, M. (2009) Chapter 2: Biogenesis of the cell wall and other glycoconjugates of Mycobacterium tuberculosis. *Advances in applied microbiology* **69**, 23-78
3. Bansal-Mutalik, R., and Nikaido, H. (2014) Mycobacterial outer membrane is a lipid bilayer and the inner membrane is unusually rich in diacyl phosphatidylinositol dimannosides. *Proc Natl Acad Sci U S A* **111**, 4958-4963
4. Barry, C. E., 3rd, Boshoff, H. I., Dartois, V., Dick, T., Ehrt, S., Flynn, J., Schnappinger, D., Wilkinson, R. J., and Young, D. (2009) The spectrum of latent tuberculosis: rethinking the biology and intervention strategies. *Nat Rev Microbiol* **7**, 845-855
5. Boshoff, H. I., and Barry, C. E., 3rd. (2005) Tuberculosis - metabolism and respiration in the absence of growth. *Nat Rev Microbiol* **3**, 70-80
6. Nathan, C., Gold, B., Lin, G., Stegman, M., de Carvalho, L. P., Vandal, O., Venugopal, A., and Bryk, R. (2008) A philosophy of anti-infectives as a guide in the search for new drugs for tuberculosis. *Tuberculosis (Edinb)* **88 Suppl 1**, S25-33
7. Rustad, T. R., Harrell, M. I., Liao, R., and Sherman, D. R. (2008) The enduring hypoxic response of Mycobacterium tuberculosis. *PLoS One* **3**, e1502
8. Rustad, T. R., Sherrid, A. M., Minch, K. J., and Sherman, D. R. (2009) Hypoxia: a window into Mycobacterium tuberculosis latency. *Cell Microbiol* **11**, 1151-1159
9. Shi, L., Sohaskey, C. D., Pfeiffer, C., Datta, P., Parks, M., McFadden, J., North, R. J., and Gennaro, M. L. (2010) Carbon flux rerouting during Mycobacterium tuberculosis growth arrest. *Mol Microbiol* **78**, 1199-1215
10. Typas, A., Banzhaf, M., Gross, C. A., and Vollmer, W. (2011) From the regulation of peptidoglycan synthesis to bacterial growth and morphology. *Nat Rev Microbiol* **10**, 123-136
11. Kramer, N. E., Smid, E. J., Kok, J., de Kruijff, B., Kuipers, O. P., and Breukink, E. (2004) Resistance of Gram-positive bacteria to nisin is not determined by lipid II levels. *FEMS Microbiol Lett* **239**, 157-161
12. Storm, D. R., and Strominger, J. L. (1974) Binding of bacitracin to cells and protoplasts of Micrococcus lysodeikticus. *J Biol Chem* **249**, 1823-1827
13. de Kruijff, B., van Dam, V., and Breukink, E. (2008) Lipid II: a central component in bacterial cell wall synthesis and a target for antibiotics. *Prostaglandins Leukot Essent Fatty Acids* **79**, 117-121
14. Breukink, E., and de Kruijff, B. (2006) Lipid II as a target for antibiotics. *Nature reviews. Drug discovery* **5**, 321-332
15. Liu, Y., and Breukink, E. (2016) The Membrane Steps of Bacterial Cell Wall Synthesis as Antibiotic Targets. *Antibiotics (Basel)* **5**
16. Ling, L. L., Schneider, T., Peoples, A. J., Spoering, A. L., Engels, I., Conlon, B. P., Mueller, A., Schaberle, T. F., Hughes, D. E., Epstein, S., Jones, M., Lazarides, L., Steadman, V. A., Cohen, D. R., Felix, C. R., Fetterman, K. A., Millett, W. P., Nitti, A. G., Zullo, A. M., Chen, C., and Lewis, K. (2015) A new antibiotic kills pathogens without detectable resistance. *Nature* **517**, 455-459
17. Elhenawy, W., Davis, R. M., Fero, J., Salama, N. R., Felman, M. F., and Ruiz, N. (2016) The O-Antigen Flippase Wzk Can Substitute for MurJ in Peptidoglycan Synthesis in Helicobacter pylori and Escherichia coli. *PLoS One* **11**, e0161587
18. Meeske, A. J., Sham, L. T., Kimsey, H., Koo, B. M., Gross, C. A., Bernhardt, T. G., and Rudner, D. Z. (2015) MurJ and a novel lipid II flippase are required for cell wall biogenesis in Bacillus subtilis. *Proc Natl Acad Sci U S A* **112**, 6437-6442
19. Boyle, D. S., Khattar, M. M., Addinall, S. G., Lutkenhaus, J., and Donachie, W. D. (1997) ftsW is an essential cell-division gene in Escherichia coli. *Molecular microbiology* **24**, 1263-1273
20. Sieger, B., Schubert, K., Donovan, C., and Bramkamp, M. (2013) The lipid II flippase RodA determines morphology and growth in Corynebacterium glutamicum. *Mol Microbiol* **90**, 966-982
21. Sham, L. T., Butler, E. K., Lebar, M. D., Kahne, D., Bernhardt, T. G., and Ruiz, N. (2014) Bacterial cell wall. MurJ is the flippase of lipid-linked precursors for peptidoglycan biogenesis. *Science* **345**, 220-222

Downloaded from http://www.jbc.org/ by guest on March 31, 2018

22. Fay, A., and Dworkin, J. (2009) Bacillus subtilis homologs of MviN (MurJ), the putative Escherichia coli lipid II flippase, are not essential for growth. *Journal of bacteriology* **191**, 6020-6028
23. Gee, C. L., Papavinasasundaram, K. G., Blair, S. R., Baer, C. E., Falick, A. M., King, D. S., Griffin, J. E., Venghatakrishnan, H., Zukauskas, A., Wei, J. R., Dhiman, R. K., Crick, D. C., Rubin, E. J., Sassetti, C. M., and Alber, T. (2012) A phosphorylated pseudokinase complex controls cell wall synthesis in mycobacteria. *Sci Signal* **5**, ra7
24. Ikeda, M., Sato, T., Wachi, M., Jung, H. K., Ishino, F., Kobayashi, Y., and Matsuhashi, M. (1989) Structural similarity among Escherichia coli FtsW and RodA proteins and Bacillus subtilis SpoVE protein, which function in cell division, cell elongation, and spore formation, respectively. *J Bacteriol* **171**, 6375-6378
25. Meeske, A. J., Riley, E. P., Robins, W. P., Uehara, T., Mekalanos, J. J., Kahne, D., Walker, S., Kruse, A. C., Bernhardt, T. G., and Rudner, D. Z. (2016) SEDS proteins are a widespread family of bacterial cell wall polymerases. *Nature*
26. Leclercq, S., Derouaux, A., Olatunji, S., Fraipont, C., Egan, A. J., Vollmer, W., Breukink, E., and Terrak, M. (2017) Interplay between Penicillin-binding proteins and SEDS proteins promotes bacterial cell wall synthesis. *Scientific reports* **7**, 43306
27. Emami, K., Guyet, A., Kawai, Y., Devi, J., Wu, L. J., Allenby, N., Daniel, R. A., and Errington, J. (2017) RodA as the missing glycosyltransferase in Bacillus subtilis and antibiotic discovery for the peptidoglycan polymerase pathway. *Nat Microbiol* **2**, 16253
28. Born, P., Breukink, E., and Vollmer, W. (2006) In vitro synthesis of cross-linked murein and its attachment to sacculi by PBP1A from Escherichia coli. *The Journal of biological chemistry* **281**, 26985-26993
29. Datta, P., Dasgupta, A., Singh, A. K., Mukherjee, P., Kundu, M., and Basu, J. (2006) Interaction between FtsW and penicillin-binding protein 3 (PBP3) directs PBP3 to mid-cell, controls cell septation and mediates the formation of a trimeric complex involving FtsZ, FtsW and PBP3 in mycobacteria. *Mol Microbiol* **62**, 1655-1673
30. Fraipont, C., Alexeeva, S., Wolf, B., van der Ploeg, R., Schloesser, M., den Blaauwen, T., and Nguyen-Disteche, M. (2011) The integral membrane FtsW protein and peptidoglycan synthase PBP3 form a subcomplex in Escherichia coli. *Microbiology* **157**, 251-259
31. Cole, S. T., Brosch, R., Parkhill, J., Garnier, T., Churcher, C., Harris, D., Gordon, S. V., Eiglmeier, K., Gas, S., Barry, C. E., 3rd, Tekaia, F., Badcock, K., Basham, D., Brown, D., Chillingworth, T., Connor, R., Davies, R., Devlin, K., Feltwell, T., Gentles, S., Hamlin, N., Holroyd, S., Hornsby, T., Jagels, K., Krogh, A., McLean, J., Moule, S., Murphy, L., Oliver, K., Osborne, J., Quail, M. A., Rajandream, M. A., Rogers, J., Rutter, S., Seeger, K., Skelton, J., Squares, R., Squares, S., Sulston, J. E., Taylor, K., Whitehead, S., and Barrell, B. G. (1998) Deciphering the biology of Mycobacterium tuberculosis from the complete genome sequence. *Nature* **393**, 537-544
32. Sharma, A. K., Arora, D., Singh, L. K., Gangwal, A., Sajid, A., Molle, V., Singh, Y., and Nandicoori, V. K. (2016) Serine/Threonine Protein Phosphatase PstP of Mycobacterium tuberculosis Is Necessary for Accurate Cell Division and Survival of Pathogen. *J Biol Chem* **291**, 24215-24230
33. Chawla, Y., Upadhyay, S., Khan, S., Nagarajan, S. N., Forti, F., and Nandicoori, V. K. (2014) Protein kinase B (PknB) of Mycobacterium tuberculosis is essential for growth of the pathogen in vitro as well as for survival within the host. *J Biol Chem* **289**, 13858-13875
34. Nagarajan, S. N., Upadhyay, S., Chawla, Y., Khan, S., Naz, S., Subramanian, J., Gandotra, S., and Nandicoori, V. K. (2015) Protein kinase A (PknA) of Mycobacterium tuberculosis is independently activated and is critical for growth in vitro and survival of the pathogen in the host. *J Biol Chem* **290**, 9626-9645
35. Kang, C. M., Abbott, D. W., Park, S. T., Dascher, C. C., Cantley, L. C., and Husson, R. N. (2005) The Mycobacterium tuberculosis serine/threonine kinases PknA and PknB: substrate identification and regulation of cell shape. *Genes Dev* **19**, 1692-1704
36. Molle, V., and Kremer, L. (2010) Division and cell envelope regulation by Ser/Thr phosphorylation: Mycobacterium shows the way. *Mol Microbiol* **75**, 1064-1077
37. Richard-Greenblatt, M., and Av-Gay, Y. (2017) Epigenetic Phosphorylation Control of Mycobacterium tuberculosis Infection and Persistence. *Microbiology spectrum* **5**

Downloaded from http://www.jbc.org/ by guest on March 31, 2018

38. Parikh, A., Kumar, D., Chawla, Y., Kurthkoti, K., Khan, S., Varshney, U., and Nandicoori, V. K. (2013) Development of a new generation of vectors for gene expression, gene replacement, and protein-protein interaction studies in mycobacteria. *Appl Environ Microbiol* **79**, 1718-1729
39. Matsuzawa, H., Asoh, S., Kunai, K., Muraiso, K., Takasuga, A., and Ohta, T. (1989) Nucleotide sequence of the rodA gene, responsible for the rod shape of Escherichia coli: rodA and the pbpA gene, encoding penicillin-binding protein 2, constitute the rodA operon. *J Bacteriol* **171**, 558-560
40. DeJesus, M. A., Gerrick, E. R., Xu, W., Park, S. W., Long, J. E., Boutte, C. C., Rubin, E. J., Schnappinger, D., Ehrt, S., Fortune, S. M., Sassetti, C. M., and Ioerger, T. R. (2017) Comprehensive Essentiality Analysis of the Mycobacterium tuberculosis Genome via Saturating Transposon Mutagenesis. *mBio* **8**
41. van Kessel, J. C., and Hatfull, G. F. (2007) Recombineering in Mycobacterium tuberculosis. *Nat Methods* **4**, 147-152
42. Begg, K. J., and Donachie, W. D. (1985) Cell shape and division in Escherichia coli: experiments with shape and division mutants. *Journal of bacteriology* **163**, 615-622
43. Wayne, L. G., and Hayes, L. G. (1996) An in vitro model for sequential study of shiftdown of Mycobacterium tuberculosis through two stages of nonreplicating persistence. *Infect Immun* **64**, 2062-2069
44. Fedarovich, A., Nicholas, R. A., and Davies, C. (2010) Unusual conformation of the SxN motif in the crystal structure of penicillin-binding protein A from Mycobacterium tuberculosis. *Journal of molecular biology* **398**, 54-65
45. Zhao, G., Meier, T. I., Kahl, S. D., Gee, K. R., and Blaszczak, L. C. (1999) BOCILLIN FL, a sensitive and commercially available reagent for detection of penicillin-binding proteins. *Antimicrob Agents Chemother* **43**, 1124-1128
46. Breukink, E., Wiedemann, I., van Kraaij, C., Kuipers, O. P., Sahl, H. G., and de Kruijff, B. (1999) Use of the cell wall precursor lipid II by a pore-forming peptide antibiotic. *Science* **286**, 2361-2364
47. Qiao, Y., Srisuknimit, V., Rubino, F., Schaefer, K., Ruiz, N., Walker, S., and Kahne, D. (2017) Lipid II overproduction allows direct assay of transpeptidase inhibition by beta-lactams. *Nature chemical biology* **13**, 793-798
48. Ostash, B., and Walker, S. (2010) Moenomycin family antibiotics: chemical synthesis, biosynthesis, and biological activity. *Nat Prod Rep* **27**, 1594-1617
49. Khan, S., Nagarajan, S. N., Parikh, A., Samantaray, S., Singh, A., Kumar, D., Roy, R. P., Bhatt, A., and Nandicoori, V. K. (2010) Phosphorylation of enoyl-acyl carrier protein reductase InhA impacts mycobacterial growth and survival. *J Biol Chem* **285**, 37860-37871
50. Jani, C., Eoh, H., Lee, J. J., Hamasha, K., Sahana, M. B., Han, J. S., Nyayapathy, S., Lee, J. Y., Suh, J. W., Lee, S. H., Rehse, S. J., Crick, D. C., and Kang, C. M. (2010) Regulation of Polar Peptidoglycan Biosynthesis by Wag31 Phosphorylation in Mycobacteria. *BMC Microbiol* **10**, 327
51. Krogh, A., Larsson, B., von Heijne, G., and Sonnhammer, E. L. (2001) Predicting transmembrane protein topology with a hidden Markov model: application to complete genomes. *J Mol Biol* **305**, 567-580
52. Stoker, N. G., Pratt, J. M., and Spratt, B. G. (1983) Identification of the rodA gene product of Escherichia coli. *Journal of bacteriology* **155**, 854-859
53. Aly, S., Wagner, K., Keller, C., Malm, S., Malzan, A., Brandau, S., Bange, F. C., and Ehlers, S. (2006) Oxygen status of lung granulomas in Mycobacterium tuberculosis-infected mice. *J Pathol* **210**, 298-305
54. Via, L. E., Lin, P. L., Ray, S. M., Carrillo, J., Allen, S. S., Eum, S. Y., Taylor, K., Klein, E., Manjunatha, U., Gonzales, J., Lee, E. G., Park, S. K., Raleigh, J. A., Cho, S. N., McMurray, D. N., Flynn, J. L., and Barry, C. E., 3rd. (2008) Tuberculous granulomas are hypoxic in guinea pigs, rabbits, and nonhuman primates. *Infect Immun* **76**, 2333-2340
55. Seiler, P., Ulrichs, T., Bandermann, S., Pradl, L., Jorg, S., Krenn, V., Morawietz, L., Kaufmann, S. H., and Aichele, P. (2003) Cell-wall alterations as an attribute of Mycobacterium tuberculosis in latent infection. *J Infect Dis* **188**, 1326-1331
56. Kieser, K. J., and Rubin, E. J. (2014) How sisters grow apart: mycobacterial growth and division. *Nat Rev Microbiol* **12**, 550-562
57. Straume, D., Stamsas, G. A., Berg, K. H., Salehian, Z., and Havarstein, L. S. (2017) Identification of pneumococcal proteins that are functionally linked to penicillin-binding protein 2b (PBP2b). *Mol Microbiol* **103**, 99-116

Downloaded from http://www.jbc.org/ by guest on March 31, 2018

58. van der Ploeg, R., Goudelis, S. T., and den Blaauwen, T. (2015) Validation of FRET Assay for the Screening of Growth Inhibitors of Escherichia coli Reveals Elongasome Assembly Dynamics. *Int J Mol Sci* **16**, 17637-17654
59. Sieger, B., and Bramkamp, M. (2014) Interaction sites of DivIVA and RodA from Corynebacterium glutamicum. *Frontiers in microbiology* **5**, 738
60. Viswanathan, G., Yadav, S., Joshi, S. V., Raghunand, T. R., and Jass, J. (2017) Insights into the function of FhaA, a cell division-associated protein in mycobacteria. *FEMS microbiology letters* **364**
61. Plocinski, P., Ziolkiewicz, M., Kiran, M., Vadrevu, S. I., Nguyen, H. B., Hugonnet, J., Veckerle, C., Arthur, M., Dziadek, J., Cross, T. A., Madiraju, M., and Rajagopalan, M. (2011) Characterization of CrgA, a new partner of the Mycobacterium tuberculosis peptidoglycan polymerization complexes. *J Bacteriol* **193**, 3246-3256
62. Cunningham, A. F., and Spreadbury, C. L. (1998) Mycobacterial stationary phase induced by low oxygen tension: cell wall thickening and localization of the 16-kilodalton alpha-crystallin homolog. *Journal of bacteriology* **180**, 801-808
63. Henriques, A. O., Glaser, P., Piggot, P. J., and Moran, C. P., Jr. (1998) Control of cell shape and elongation by the rodA gene in Bacillus subtilis. *Molecular microbiology* **28**, 235-247
64. Costa, C. S., and Anton, D. N. (1999) Conditional lethality of cell shape mutations of Salmonella typhimurium: rodA and mre mutants are lethal on solid but not in liquid medium. *Curr Microbiol* **38**, 137-142
65. Mohammadi, T., Sijbrandi, R., Lutters, M., Verheul, J., Martin, N. I., den Blaauwen, T., de Kruijff, B., and Breukink, E. (2014) Specificity of the transport of lipid II by FtsW in Escherichia coli. *The Journal of biological chemistry* **289**, 14707-14718
66. McPherson, D. C., and Popham, D. L. (2003) Peptidoglycan synthesis in the absence of class A penicillin-binding proteins in Bacillus subtilis. *Journal of bacteriology* **185**, 1423-1431
67. Sureka, K., Hossain, T., Mukherjee, P., Chatterjee, P., Datta, P., Kundu, M., and Basu, J. (2010) Novel role of phosphorylation-dependent interaction between FtsZ and FipA in mycobacterial cell division. *PLoS One* **5**, e8590
68. Thakur, M., and Chakraborti, P. K. (2008) Ability of PknA, a mycobacterial eukaryotic-type serine/threonine kinase, to transphosphorylate MurD, a ligase involved in the process of peptidoglycan biosynthesis. *Biochem J* **415**, 27-33
69. Soni, V., Upadhayay, S., Suryadevara, P., Samla, G., Singh, A., Yogeeswari, P., Sriram, D., and Nandicoori, V. K. (2015) Depletion of M. tuberculosis GlmU from Infected Murine Lungs Effects the Clearance of the Pathogen. *PLoS Pathog* **11**, e1005235
70. Kieser, K. J., Boutte, C. C., Kester, J. C., Baer, C. E., Barczak, A. K., Meniche, X., Chao, M. C., Rego, E. H., Sassetti, C. M., Fortune, S. M., and Rubin, E. J. (2015) Phosphorylation of the Peptidoglycan Synthase PonA1 Governs the Rate of Polar Elongation in Mycobacteria. *PLoS Pathog* **11**, e1005010
71. Nakedi, K. C., Nel, A. J., Garnett, S., Blackburn, J. M., and Soares, N. C. (2015) Comparative Ser/Thr/Tyr phosphoproteomics between two mycobacterial species: the fast growing Mycobacterium smegmatis and the slow growing Mycobacterium bovis BCG. *Frontiers in microbiology* **6**, 237
72. Yang, D. C., Blair, K. M., and Salama, N. R. (2016) Staying in Shape: the Impact of Cell Shape on Bacterial Survival in Diverse Environments. *Microbiol Mol Biol Rev* **80**, 187-203
73. Doerks, T., van Noort, V., Minguez, P., and Bork, P. (2012) Annotation of the M. tuberculosis hypothetical orfeome: adding functional information to more than half of the uncharacterized proteins. *PloS one* **7**, e34302
74. van Teeseling, M. C. F., de Pedro, M. A., and Cava, F. (2017) Determinants of Bacterial Morphology: From Fundamentals to Possibilities for Antimicrobial Targeting. *Frontiers in microbiology* **8**, 1264
75. Boutte, C. C., Baer, C. E., Papavinasasundaram, K., Liu, W., Chase, M. R., Meniche, X., Fortune, S. M., Sassetti, C. M., Ioerger, T. R., and Rubin, E. J. (2016) A cytoplasmic peptidoglycan amidase homologue controls mycobacterial cell wall synthesis. *Elife* **5**
76. Vandal, O. H., Nathan, C. F., and Ehrt, S. (2009) Acid resistance in Mycobacterium tuberculosis. *J Bacteriol* **191**, 4714-4721

Downloaded from http://www.jbc.org/ by guest on March 31, 2018

77. Pang, X., Vu, P., Byrd, T. F., Ghanny, S., Soteropoulos, P., Mukamolova, G. V., Wu, S., Samten, B., and Howard, S. T. (2007) Evidence for complex interactions of stress-associated regulons in an mprAB deletion mutant of Mycobacterium tuberculosis. *Microbiology* **153**, 1229-1242
78. Manganelli, R., Voskuil, M. I., Schoolnik, G. K., and Smith, I. (2001) The Mycobacterium tuberculosis ECF sigma factor sigmaE: role in global gene expression and survival in macrophages. *Molecular microbiology* **41**, 423-437
79. Manganelli, R., Voskuil, M. I., Schoolnik, G. K., Dubnau, E., Gomez, M., and Smith, I. (2002) Role of the extracytoplasmic-function sigma factor sigma(H) in Mycobacterium tuberculosis global gene expression. *Molecular microbiology* **45**, 365-374
80. Dahl, J. L., Kraus, C. N., Boshoff, H. I., Doan, B., Foley, K., Avarbock, D., Kaplan, G., Mizrahi, V., Rubin, H., and Barry, C. E., 3rd. (2003) The role of RelMtb-mediated adaptation to stationary phase in long-term persistence of Mycobacterium tuberculosis in mice. *Proceedings of the National Academy of Sciences of the United States of America* **100**, 10026-10031
81. Klinkenberg, L. G., Lee, J. H., Bishai, W. R., and Karakousis, P. C. (2010) The stringent response is required for full virulence of Mycobacterium tuberculosis in guinea pigs. *The Journal of infectious diseases* **202**, 1397-1404
82. Tsai, M. C., Chakravarty, S., Zhu, G., Xu, J., Tanaka, K., Koch, C., Tufariello, J., Flynn, J., and Chan, J. (2006) Characterization of the tuberculous granuloma in murine and human lungs: cellular composition and relative tissue oxygen tension. *Cell Microbiol* **8**, 218-232
83. Emori, K., and Tanaka, A. (1978) Granuloma formation by synthetic bacterial cell wall fragment: muramyl dipeptide. *Infect Immun* **19**, 613-620
84. Pandey, A. K., Raman, S., Proff, R., Joshi, S., Kang, C. M., Rubin, E. J., Husson, R. N., and Sassetti, C. M. (2009) Nitrile-inducible gene expression in mycobacteria. *Tuberculosis (Edinb)* **89**, 12-16
85. Wei, J. R., Krishnamoorthy, V., Murphy, K., Kim, J. H., Schnappinger, D., Alber, T., Sassetti, C. M., Rhee, K. Y., and Rubin, E. J. (2011) Depletion of antibiotic targets has widely varying effects on growth. *Proc Natl Acad Sci U S A* **108**, 4176-4181
86. Sajid, A., Arora, G., Gupta, M., Upadhyay, S., Nandicoori, V. K., and Singh, Y. (2011) Phosphorylation of Mycobacterium tuberculosis Ser/Thr phosphatase by PknA and PknB. *PLoS One* **6**, e17871
87. Parker, A. E., and Bermudez, L. E. (1997) Expression of the green fluorescent protein (GFP) in mycobacterium avium as a tool to study the interaction between Mycobacteria and host cells. *Microb Pathog* **22**, 193-198
88. Jain, P., Hsu, T., Arai, M., Biermann, K., Thaler, D. S., Nguyen, A., Gonzalez, P. A., Tufariello, J. M., Kriakov, J., Chen, B., Larsen, M. H., and Jacobs, W. R., Jr. (2014) Specialized transduction designed for precise high-throughput unmarked deletions in Mycobacterium tuberculosis. *MBio* **5**, e01245-01214
89. Khan, M. Z., Bhaskar, A., Upadhyay, S., Kumari, P., Rajmani, R. S., Jain, P., Singh, A., Kumar, D., Bhavesh, N. S., and Nandicoori, V. K. (2017) Protein Kinase G confers survival advantage to Mycobacterium tuberculosis during latency like conditions. *J Biol Chem*
90. Martin, A., Camacho, M., Portaels, F., and Palomino, J. C. (2003) Resazurin microtiter assay plate testing of Mycobacterium tuberculosis susceptibilities to second-line drugs: rapid, simple, and inexpensive method. *Antimicrobial agents and chemotherapy* **47**, 3616-3619
91. Miesel, L., Weisbrod, T. R., Marcinkeviciene, J. A., Bittman, R., and Jacobs, W. R., Jr. (1998) NADH dehydrogenase defects confer isoniazid resistance and conditional lethality in Mycobacterium smegmatis. *Journal of bacteriology* **180**, 2459-2467
92. Patru, M. M., and Pavelka, M. S., Jr. (2010) A role for the class A penicillin-binding protein PonA2 in the survival of Mycobacterium smegmatis under conditions of nonreplication. *J Bacteriol* **192**, 3043-3054
93. Dephoure, N., and Gygi, S. P. (2011) A solid phase extraction-based platform for rapid phosphoproteomic analysis. *Methods* **54**, 379-386
94. Jhingan, G. D., Kumari, S., Jamwal, S. V., Kalam, H., Arora, D., Jain, N., KrishnaKumaar, L., Samal, A., Rao, K. V., Kumar, D., and Nandicoori, V. K. (2016) Comparative proteomic analyses of avirulent, virulent and clinical strains of Mycobacterium tuberculosis identifies strain-specific patterns. *J Biol Chem*
95. Parikh, A., Verma, S. K., Khan, S., Prakash, B., and Nandicoori, V. K. (2009) PknB-mediated phosphorylation of a novel substrate, N-acetylglucosamine-1-phosphate uridyltransferase, modulates its acetyltransferase activity. *J Mol Biol* **386**, 451-464

Downloaded from http://www.jbc.org/ by guest on March 31, 2018

FIGURE LEGENDS

Figure 1. Schematic diagram depicting the enzymes catalyzing multiple steps of Peptidoglycan biosynthesis pathway and the stages at which PG biosynthesis inhibitors act. Pathway was drawn with the help of ChemDraw Ultra 12.0 software.

Figure 2: ***Overexpression of RodA and PbpA leads to cell elongation in Mtb.*** **a.** Pictorial representation of the operon encoding *rodA and pbpA*. Upstream serine/threonine phosphatase, *pstp* and downstream serine/threonine kinase genes, *pknA* and *pknB* are indicated. **b.** Fresh cultures of *Mtb::Vc (vector control)* or *Mtb::rodA or Mtb::pbpA* were seeded at an initial A_{600} of 0.1 in either 7H9 (Upper Panel); or Sauton's medium (Lower Panel); in presence of 100 ng/ml ATc and cells were allowed to grow for 6 days at 37°C at 100 rpm and fixed. Morphology of *Mtb::Vc , Mtb::rodA* and *Mtb::pbpA* were observed through scanning electron microscopy at 20000X. Scale bar, 1.0 μm. **c.** Quantification of cell lengths in *Mtb::Vc , Mtb*::*rodA* and *Mtb*::*pbpA* strains (n: ~200) from cells grown in 7H9 medium (Left Panel) or Sauton's medium (Right Panel). Mean cell lengths obtained are *Mtb::Vc*-1.9 μm, *Mtb::rodA*-2.34 μm and *Mtb::pbpA*-2.18 μm in 7H9 media and *Mtb::Vc*-2.1 μm, *Mtb::rodA*-2.8 μm and *Mtb::pbpA*-2.8 μm for Sauton's media. Cell lengths were measured independently using Smart Tiff software and plotted scattered dot plot with mean values using GraphPad Prism6. The experiments were biologically and technically repeated thrice. Statistical analysis was performed with the help of One way ANOVA test. ****, P<.0001.

Figure 3. Generation of rodA, pbpA and rodA-pbpA gene replacement mutants in Mtb. **a.** Schematic depiction of strategy used for the generation of gene deletion mutants. Primers used for the PCR confirmation are indicated. **b.** Genomic DNA was isolated from log cultures of wild type and mutants and PCR reactions were performed with defined set of primers (as indicated). Lane1; Mr-1 kb ladder; lane 2: *Mtb;* lane3: *MtbΔr*; lane 4: *MtbΔp* and lane 5: *MtbΔrp*. Expected size for the F1 and R1 pair are *Mtb*-1410 bp; *MtbΔr* -1300bp; *MtbΔp* -1410 bp and *MtbΔrp*- nil. Expected size for the F2 and R2 pair are *Mtb*-1476 bp; *MtbΔr*-1476 bp; *MtbΔp* -1300bp and *MtbΔrp*-nil. Expected size for the F1 and R2 pair are *Mtb*-2886 bp; *MtbΔr*-2726 bp; *MtbΔp* -2660bp and *MtbΔrp*-1300**. c.** Western blots analysis to detect polarity effects in deletion mutants *Mtb, MtbΔr, MtbΔp* and *MtbΔrp* strains. Strains were grown to an A_{600} of 0.8 – 1.0 and whole cell lysates (WCLs) were resolved and probed with α-PstP, α-PknA, α-PknB, and α-GroEL-I antibodies. **d-e.** *Mtb*, *MtbΔr, MtbΔp* and *MtbΔrp* strains were inoculated at A_{600}~ 0.1 in 7H9 or Sauton's medium and growth was monitored as bacterial survival by CFU enumeration at indicated time points for 7H9**(d)** and Sauton's**(e)**. Experiment was performed in triplicate and the results were plotted using GraphPad Prism6. Error bars indicate standard deviation (SD).

Figure 4. RodA and PbpA play independent roles in modulating bacterial cell length. **a-b.** Fresh cultures of *Mtb, MtbΔr, MtbΔp, MtbΔrp* were seeded at an initial A_{600} of 0.1 and grown for 6 days at 37°C at 100 rpm in 7H9 or Sauton's medium followed by fixation. Morphology of the cells were observed through scanning electron microscopy at 20000X for **(a)** 7H9 and **(b)** Sauton's media. Scale bar, 2.0 μm. **c.** Quantification of cell lengths (n: ~200) of *Mtb, MtbΔr, MtbΔp, MtbΔrp* strains cells grown in 7H9 medium was performed. Cell lengths were measured independently using Smart Tiff software and plotted scattered dot plot with mean values using GraphPad Prism6. Mean cell lengths obtained are: *Mtb*-2.1 μm, *MtbΔr*-1.5 μm, *MtbΔp*-2.0 μm and *MtbΔrp*-2.3 μm. The experiments were biologically and technically repeated twice. Cell lengths were analyzed using GraphPad Prism6 and statistical analysis was performed using One way ANOVA test, ****, P<.0001; ***, P<.001; ns: not significant. **d.** Quantification of cell lengths in *Mtb, MtbΔr, MtbΔp, MtbΔrp* strains (n: ~200) cells grown in Sauton's medium was performed and Mean cell lengths obtained are: *Mtb*-2.3 μm, *MtbΔr*-1.8 μm, *MtbΔp*-2.7 μm and *MtbΔrp*-2.6 μm. The experiments were biologically and technically repeated twice. Cell lengths were measured independently using Smart Tiff

Downloaded from http://www.jbc.org/ by guest on March 31, 2018

software and plotted scattered dot plot with mean values using GraphPad Prism6 and the statistical analysis was performed with One way ANOVA test, ****, P<.0001; ***, P<.001. **e.** Fresh cultures of *Mtb, MtbΔr, MtbΔp, MtbΔrp* were seeded at an initial A_{600} of 0.1 and grown at 37°C at 100 rpm in Sauton's medium followed by fixation at different time points (day 0, day 3, day 6 and day 9) of growth and cell lengths were measured as described above. Mean cell lengths obtained for different time points are: Day 0: *Mtb*-1.98 μm, *MtbΔr*-1.80 μm, *MtbΔp*-1.84 μm and *MtbΔrp*-1.76 μm; Day3 *Mtb*-2.87 μm, *MtbΔr*-2.26 μm, *MtbΔp*-2.69 μm and *MtbΔrp*-2.62 μm; Day6 *Mtb*-2.72 μm, *MtbΔr*-2.32 μm, *MtbΔp*-2.92 μm and *MtbΔrp*-2.90 μm and Day9 *Mtb*-2.71 μm, *MtbΔr*-2.0 μm, *MtbΔp*-2.91 μm and *MtbΔrp*-2.88 μm. Cell lengths were analyzed using GraphPad Prism6 and statistical analysis was performed using One way ANOVA test, ****, P<.0001; ***, P<.001; **, P<.01; ns: not significant. **f.** Fresh cultures of *Mtb* or *MtbΔr or MtbΔr::r or MtbΔp or MtbΔp::p* were seeded at an initial A_{600} of 0.1 in Sauton's medium and continued to grow for 6 days in presence of 0.1 μM IVN and cells were fixed and processed for SEM. Cell lengths were observed through SEM at 20000X. Cell lengths were measured as described above. Obtained mean cell lengths were: *Mtb*-2.1μm, *MtbΔr*-1.9μm *and MtbΔr::r*-2.5μm, *MtbΔp*-3.1 *and MtbΔp::p*-2.5 μm. Statistical analysis was performed using Two way ANOVA test, ****, P<.0001; **, P<.01.

Figure 5. Deciphering the roles of rodA and pbpA in mycobacterial cell fitness. **a-d.** Transmission electron microscopy (TEM) analysis of *Mtb rodA* and *pbpA* deletion mutants in 7H9 **(a,c)** or Sauton's medium**(b,d)**. Fresh cultures of *Mtb, MtbΔr, MtbΔp, MtbΔrp* were seeded at an initial A_{600} of 0.1 and grown for 6 days at 37°C at 100 rpm in 7H9 or Sauton's medium followed by fixation. Fixed cells were processed for TEM and cell wall architecture was observed at 200 kV, 50000X **(a)** 7H9 and **(b)** Sauton's. **c-d.** Quantification of cell wall thickness in *MtbΔr, MtbΔp, MtbΔrp* strains (n=6-7) grown in (**c)** 7H9 medium (mean cell wall thickness-*Mtb*, *MtbΔr, MtbΔp*-17 nm and *MtbΔrp*-20.2 nm. **(d)** Sauton's medium (mean cell wall thickness-*Mtb*-18 nm; *MtbΔr*-15.9 nm; *MtbΔp*-28.7 nm and *MtbΔrp*-30.6 nm. Cell wall thickness was measured independently using SmartTiff software and analysed using GraphPad Prism6 and statistical analysis was performed using Two way ANOVA test, ****, P<.0001; ***, P<.001. Red bars indicate cell wall thickness**. e-f.** Hypoxia and persisters analysis for *Mtb* and *Msm* deletion mutants (**e)** Bacterial survival analysis of day 42 post hypoxia (Wayne model) for *Mtb, MtbΔr* and *MtbΔp*. Results were plotted using GraphPad prism 6. Error bar presents standard deviation. Statistical analysis was performed using 2 tailed test; *, P<0.05. Similar results were obtained in two independent experiments performed in duplicates. (**f**) Persisters analysis of *Msm, MsmΔr* and *MsmΔp*: Cultures were grown till exponential phase and treated with 10 μg/ml isoniazid for 48 h and CFU obtained pre-and post isoniazid treatment were plotted. Statistical analysis was performed using 2 tailed test, **, P<0.005. Error bar presents standard deviation. Similar results were obtained in two independent experiments performed in triplicates.

Figure 6. RodA functions as a non-canonical transglycosylase and PbpA as a classical transpeptidase. **a.** MIC analysis of *Msm, MsmΔr* and *MsmΔp was* performed as described in methods. Graph represents the fold difference with respect to *Msm* in (CFU x MIC) values obtained for *MsmΔr* and *MsmΔp*. The experiment is performed in triplicates. **b.** MIC_{99} analysis for *MsmΔp* complementation studies: Tabular representation of MIC_{99} values obtained upon REMA assay performed with *Msm, MsmΔp, MsmΔp::p* strains in Dubo's media for oxacillin +clavulanic acid, vancomycin and isoniazid. **c.** Membrane fractions were prepared from cultures of *Msm, MsmΔp, MsmΔp::p MsmΔp::*p_{S281A} and *MsmΔp::*p_{K424G} induced with 5μM IVN. ~20 μg of membrane was incubated with Bocillin FL and resolved on 8% SDS-PAGE, and Bocillin-labeled proteins was detected using Typhoon Scanner. Similar amount of membrane extracts were processed for immunoblot analysis. Bands corresponding to endogenous PbpA and episomal 3X-FLAG-$PbpA_{wt/mut}$ are indicated. **d.** *Msm* and *MsmΔr strains* grown in Sauton's media till A_{600}~0.2-0.3 were

Downloaded from http://www.jbc.org/ by guest on March 31, 2018

pulsed with ^{3}H-mDAP and equal amounts of cultures were processed for small-scale LipidII accumulation analysis. Radiolabeled ^{3}H-LipidII in the samples was quantified. Reading obtained for *Msm* in each independent experiment was normalized to 100% and the counts obtained for *MsmΔr* were represented as percent change with respect to counts obtained for *Msm*. The experiment was performed in biological triplicates. Statistical analysis was performed using 2 tailed test; ***, P<0.0005. **e.** REMA assay for *Msm, MsmΔr, MsmΔr::r$_{mtb}$, MsmΔr::r$_{msm}$, MsmΔr::ftsW* and *MsmΔr::mviN* for isoniazid and moenomycin. The experiment was performed in triplicates and a representative data set is shown. **f.** Growth analysis of *Msm, MsmΔr, MsmΔr::r$_{mtb}$, MsmΔr:: rmsm, MsmΔr::ftsW* and *MsmΔr::mviN,* streaked on 7H11 in presence or absence of 1 μg/ml moenomycin. The experiment was performed in triplicates and a representative data set is shown.

Figure 7. Amino acid residues critical for non-canonical transglycosylase function are conserved in mycobacterial RodA. **a.** Schematic depicting the organization of RodA across the membrane. Both N and C-terminus are predicted to be inside the cytoplasm with 12 transmembrane domains by TMHMM. Residues suggested to be critical for transglycoylase activity W175 and D343 are marked. **b.** Growth analysis of *Msm, MsmΔr, MsmΔr::r$_{Mtb}$, MsmΔr::r$_{Mtb\text{-}W175R}$, MsmΔr::r$_{Mtb\text{-}D343R}$* and *MsmΔr::r$_{Mtb\text{-}DM,}$* streaked on 7H11 plates in presence or absence of 1 μg/ml moenomycin **c.** Growth analysis of *Msm, MsmΔr, MsmΔr::r$_{Msm}$, MsmΔr::r$_{Msm\text{-}W176R}$, MsmΔr::r$_{Msm\text{-}D344R}$* and *MsmΔr::r$_{Msm\text{-}DM,}$* streaked on 7H11 plates in presence or absence of 1 μg/ml moenomycin. **d.** REMA assay for *Msm, MsmΔr, MsmΔr::r$_{Mtb}$, MsmΔr::r$_{Msm,}$ MsmΔr::r$_{Mtb\text{-}W175R}$, MsmΔr::r$_{Mtb\text{-}D343R,}$ MsmΔr::r$_{Msm\text{-}W176R}$, MsmΔr::r$_{Msm\text{-}D344R}$* and *MsmΔr::r$_{Mtb\text{-}DM}$* and *MsmΔr::r$_{Msm\text{-}DM}$* for isoniazid and moenomycin. The experiment was performed in triplicates and a representative data set is shown.

Figure 8. RodA is phosphorylated on T463 residue. **a.** MS/MS spectrum of precursor m/z: 761.88025 (+2) and MH+: 1522.75322 Da, of the phosphopeptide SPITAAG(pT)EVIERV. Location of T_{463} was evident by the presence of ion series containing y_6, y_7, b_3, b_7 and $y_{8\text{-}11}$ in the spectra**. b-c. (b).** Coomassie-stained purified MBP-STPKs and His-FLAG-RodA$_{411\text{-}469.}$ **(c)** *In vitro* kinase assay was performed with 10 pmoles of MBP-STPKs and 312 pmoles of His-FLAG-RodA$_{411\text{-}469}$. Samples were resolved on 15% SDS-PAGE, stained with coomassie (bottom panel) and autoradiographed (top panel). **(d)** Fresh cultures of *Mtb*, or *MtbΔr, or MtbΔr::r, or MtbΔr::r$_{T463A}$ or MtbΔr::r$_{T463E}$* were seeded at an initial A_{600} of 0.1 in 7H9 medium and continued to grow for 6 days in presence of 100 ng of ATc. followed by fixation. SEM was performed to analyze the morphology of the cells (20,000X). Scale bar, 2 μm. **(e)** Cell lengths of ~ 200 individual cells for each sample were quantified. Mean cell length for the samples were; *Mtb* -2.1 μm*, MtbΔr*- 1.6 μm*, MtbΔr::r*- 2.5 μm*, MtbΔr::r$_{T463A}$*-1.8 μm *and MtbΔr::r$_{T463E}$*- 2.2 μm. Similar results were obtained in a biological replicate. Statistical analysis was performed using One way ANOVA test, ****, P<.0001; ***, P<.001.

Figure 9. RodA and PbpA are important for pathogen survival in the host. **a.** Five mice/group/time point were aerosolically infected with 200 CFU/ lung of *Mtb, MtbΔr, MtbΔp* and *MtbΔrp* strains. CFUs were enumerated in the lungs of infected mice after day 1 (4 mice/group), one, two, four and eight weeks (five mice /group) post infection. **b-d.** Five guinea pigs/group/ time point were infected with *Mtb, MtbΔr, MtbΔp* and *MtbΔrp* strains, animals were sacrificed at 4-week post-infection. **b.** Representative images for gross assessment of lungs and spleen from infected guinea pigs four weeks post infection. Discrete tubercles in the lungs were shown with white arrows. **c & d.** CFUs enumeration from the infected lungs **(c)** and spleen **(d)**. Mean CFU values in the lungs of guinea pigs **(c)** infected with *Mtb, MtbΔr, MtbΔp* and *Mtbrp* were 4.51, 4.2, 3.54 and 3.81 on $\log_{10}$ scale, respectively. Statistical analysis was performed using One way ANOVA test. ****, P<.0001; **, P<.01. Mean CFU values in the spleens of guinea pigs **(d)** infected with *Mtb, MtbΔr, MtbΔp* and *Mtb* were 3.44, 3.41, 3.39 and 3.54 on $\log_{10}$ scale, respectively.

Downloaded from http://www.jbc.org/ by guest on March 31, 2018

Figure 10. RodA and PbpA mutants show compromised granulomatus pathology in the host. **a.** Representative 40 X and 400 X images (upper panel) of H&E-stained lung sections obtained from guinea pigs infected with *Mtb* or *MtbΔr* or *MtbΔp* or *MtbΔrp* at 4-week post infection. 400 X images (lower panel) of H&E-stained spleen sections obtained from guinea pigs infected with *Mtb* or *MtbΔr* or *MtbΔp* or *MtbΔrp* at 4 week post infection, G, granuloma; AS, alveolar spaces; FC, foamy histiocytic cells. **b-d.** Granuloma score analysis: Scatter plot of the granuloma scores obtained (calculated as described in materials and methods) of all animals for H&E-stained lung **(b)** and spleen **(c)** sections of guinea pigs. Each data point represents score of an individual animal(n=5), statistical analysis was performed using One way ANOVA test. **, P<.01**. (d)** Tabular presentation of granuloma scores of H&E-stained lung and spleen sections for each group showing types of granuloma observed, calculation of granuloma score and the total granuloma score obtained 4 weeks post infection.

Downloaded from http://www.jbc.org/ by guest on March 31, 2018

Table 1: *MIC$_{99}$ values in µg/ml*

a.

Strain	MIC$_{99}$ Vancomycin	MIC$_{99}$ Nisin	MIC$_{99}$ Oxacillin +Clavulanic Acid	MIC$_{99}$ Moenomycin	MIC$_{99}$ Isoniazid
Msm	2.5-1.25	100-50	250-125	3.1	5.0-2.50
MsmΔr	0.162-0.15	25-12.5	≤31.25	0.18	2.5-1.25
MsmΔp	0.625	50-25	≤31.25	0.75	2.5-1.25
MsmΔrp	0.3125	25-12.5	≤31.25	0.37	2.5-1.25

b.

Strain	MIC$_{99}$ Moenomycin	MIC$_{99}$ Vancomycin	MIC$_{99}$ Nisin	MIC$_{99}$ Isoniazid
Msm	1.5	0.62	100	2.5
MsmΔr	0.18	0.15	50	2.5
MsmΔr::r$_{mtb}$	0.75	0.31	50	2.5
MsmΔr::r$_{msm}$	0.75	0.31	100	5.0
MsmΔr::ftsW	0.18	0.15	50	2.5
MsmΔr::mviN	0.18	0.15	50	2.5
MsmΔr::r$_{mtb}$-W175R	0.18	0.15	50	2.5
MsmΔr::r$_{mtb}$-D343R	0.37	0.15	50	2.5
MsmΔr::r$_{mtb}$-DM	0.18	0.15	50	2.5
MsmΔr::r$_{msm}$-W176R	0.18	0.15	50	2.5
MsmΔr::r$_{msm}$-D344R	0.18	0.15	50	2.5
MsmΔr::r$_{msm}$-DM	0.18	0.15	50	2.5

Downloaded from http://www.jbc.org/ by guest on March 31, 2018

Table 2: List of constructs and strains used in the study

Constructs	**Description**
pENTRCm^r	pENTR chloramphenicol cloned in KpnI and SnaBI amplified from pVR1
pNit1 (84)	Nitrile inducible vector *kan^r*
pNit^{chl}	pNit1 vector modified by inserting *cm^r* gene
pST-KT (38)	Anhydrotetracyclin inducible vector (ref) *kan^r*
pJV53 (41)	Plasmid encoding phage phage Che9c *60* and *61* genes under acetamide-inducible promoter; *kan^r*
pNit-ET (85)	Plasmid encoding phage Che9c *60* and *61* genes cloned in pNit1; *kan^r*
Strains	**Description**
DH5α	*E. coli* strain used for cloning experiments
Msm	Wild type *M. smegmatis mc^{2}155* strain
Mtb	Wild type H37Rv *M. tuberculosis* strain
Mtb::*Vc*	*Mtb* electroporated with pST-KT; *kan^r*
Mtb::*rodA*	*Mtb* electroporated with pST-KT-RodA$_{Mtb}$; *kan^r*
Mtb::*pbpA*	*Mtb* electroporated with pST-KT-PbpA$_{Mtb}$; *kan^r*
Mtb::*pNitET*	*Mtb* electroporated with pNit-ET; *kan^r*
MtbΔr	*rodA$_{Mtb}$* gene replacement mutant; *hyg^r*
MtbΔp	*pbpA$_{Mtb}$* gene replacement mutant; *hyg^r*
MtbΔrp	*rodA$_{Mtb}$-pbpA$_{Mtb}$* gene replacement mutant; *hyg^r*
MtbΔr::r	*MtbΔr* complemented with pNit^{chl}-RodA$_{Mtb}$; *hyg^r*, *cm^r*
MtbΔp::p	*MtbΔp* complemented with pNit^{chl}-PbpA$_{Mtb}$; *hyg^r*, *cm^r*
MtbΔr::r	*MtbΔr* complemented with pST-KT-RodA$_{Mtb}$; *hyg^r*, *kan^r*
MtbΔr::r$_{T463A}$	*MtbΔr* complemented with pST-KT-RodA$_{Mtb-T463A}$; *hyg^r*, *kan^r*
MtbΔr::r$_{T463E}$	*MtbΔr* complemented with pST-KT-RodA$_{Mtb-T463E}$; *hyg^r*, *kan^r*
Msm::pJV53	*Msm* electroporated with pJV53 plasmid; *kan^r*
MsmΔr	*Msm rodA* gene replacement mutant; *hyg^r*
MsmΔp	*Msm pbpA* gene replacement mutant; *hyg^r*
MsmΔrp	*Msm rodA-pbpA* gene replacement mutant; *hyg^r*
Msm::pN	*Msm* electroporated with pNit^{chl}; *cm^r*
Msm::pN-r	*Msm* electroporated with pNit^{chl}-RodA$_{Mtb}$; *cm^r*
Msm::pN-*p*	*Msm* electroporated with pNit^{chl}-PbpA; *cm^r*
MsmΔp::p$_{Mtb}$	*MsmΔp* complemented with pST-KT-PbpA$_{Mtb}$; *hyg^r*, *kan^r*
MsmΔp::p	*MsmΔp* electroporated with pNit-PbpA; *hyg^r*, *kan^r*
MsmΔp::p$_{S281A}$	*MsmΔp* electroporated with pNit-PbpA$_{S281A}$; *hyg^r*, *kan^r*
MsmΔp::p$_{K424G}$	*MsmΔp* electroporated with pNit-PbpA$_{K424G}$; *hyg^r*, *kan^r*
MsmΔr::r$_{Mtb}$	*MsmΔr* complemented with pST-KT-RodA$_{Mtb}$; *hyg^r*, *kan^r*
MsmΔr::r$_{Msm}$	*MsmΔr* complemented with pST-KT-RodA$_{Msm}$; *hyg^r*, *kan^r*
MsmΔr::ftsW	*MsmΔr* complemented with pST-KT-FtsW$_{Mtb}$; *hyg^r*, *kan^r*
MsmΔr::mviN	*MsmΔr* complemented with pST-KT-MviN$_{Mtb}$; *hyg^r*, *kan^r*
MsmΔp::p$_{Mtb}$	*MsmΔp* complemented with pST-KT-PbpA$_{Mtb}$; *hyg^r*, *kan^r*
MsmΔr::r$_{Mtb}$-W175R	*MsmΔr* complemented with pST-KT-RodA$_{Mtb-W175R}$; *hyg^r*, *kan^r*
MsmΔr::r$_{Mtb}$-D343R	*MsmΔr* complemented with pST-KT-RodA$_{Mtb-D343R}$; *hyg^r*, *kan^r*
MsmΔr::r$_{Mtb}$-DM	*MtbΔr* complemented with pST-KT-RodA$_{Mtb- W175R -D343R}$; *hyg^r*, *kan^r*
MsmΔr::r$_{Msm}$-W176R	*MtbΔr* complemented with pST-KT-RodA$_{Msm-W176R}$; *hyg^r*, *kan^r*
MsmΔr::r$_{Msm}$-D344R	*MtbΔr* complemented with pST-KT-RodA$_{Msm-D344R}$; *hyg^r*, *kan^r*
MsmΔr::r$_{Msm}$-DM	*MtbΔr* complemented with pST-KT-RodA$_{Msm- W176R -D344R}$; *hyg^r*, *kan^r*

Downloaded from http://www.jbc.org/ by guest on March 31, 2018

Figure 1

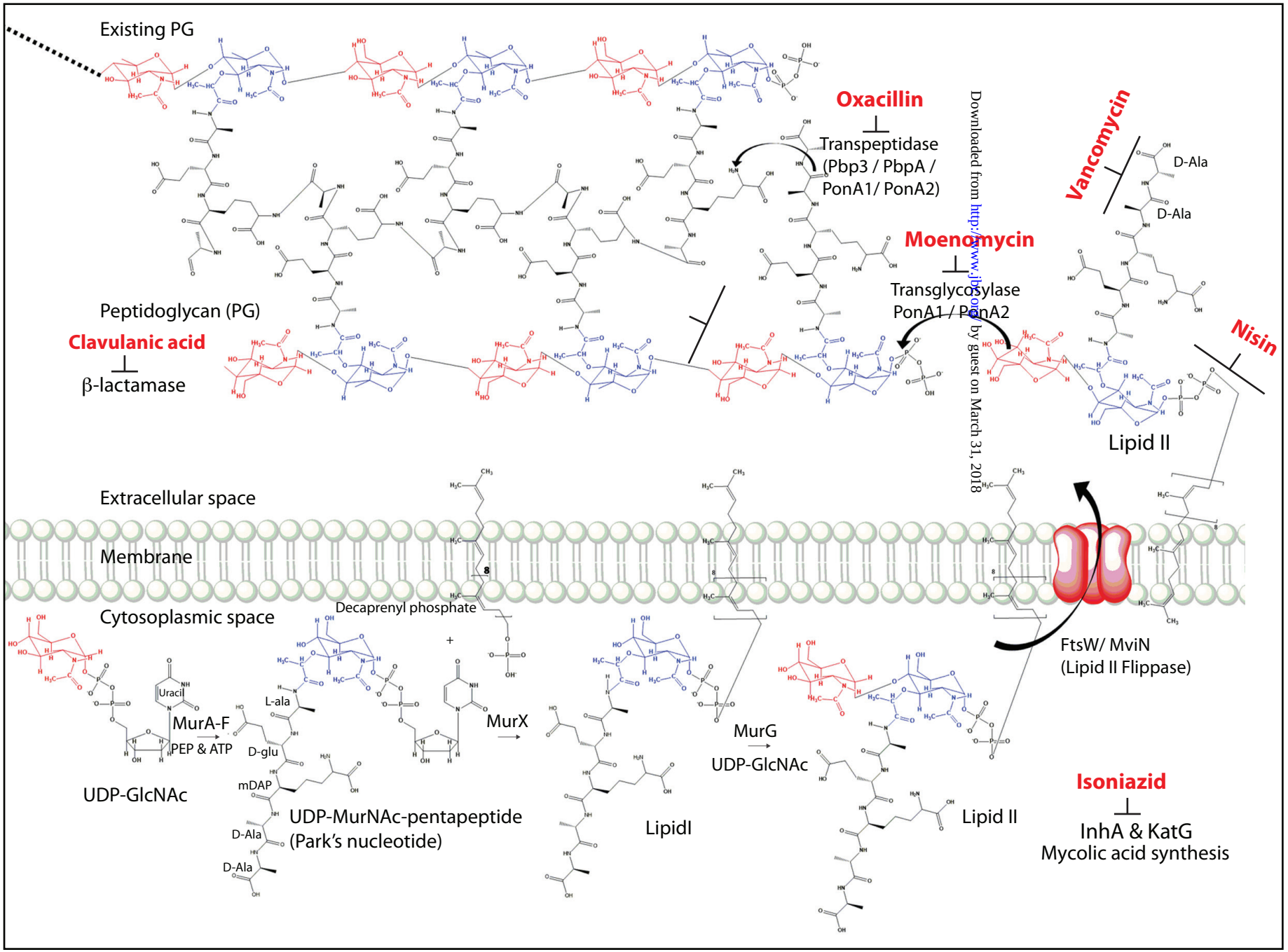

Downloaded from http://www.jb.asm.org/ by guest on March 31, 2018

Figure 2

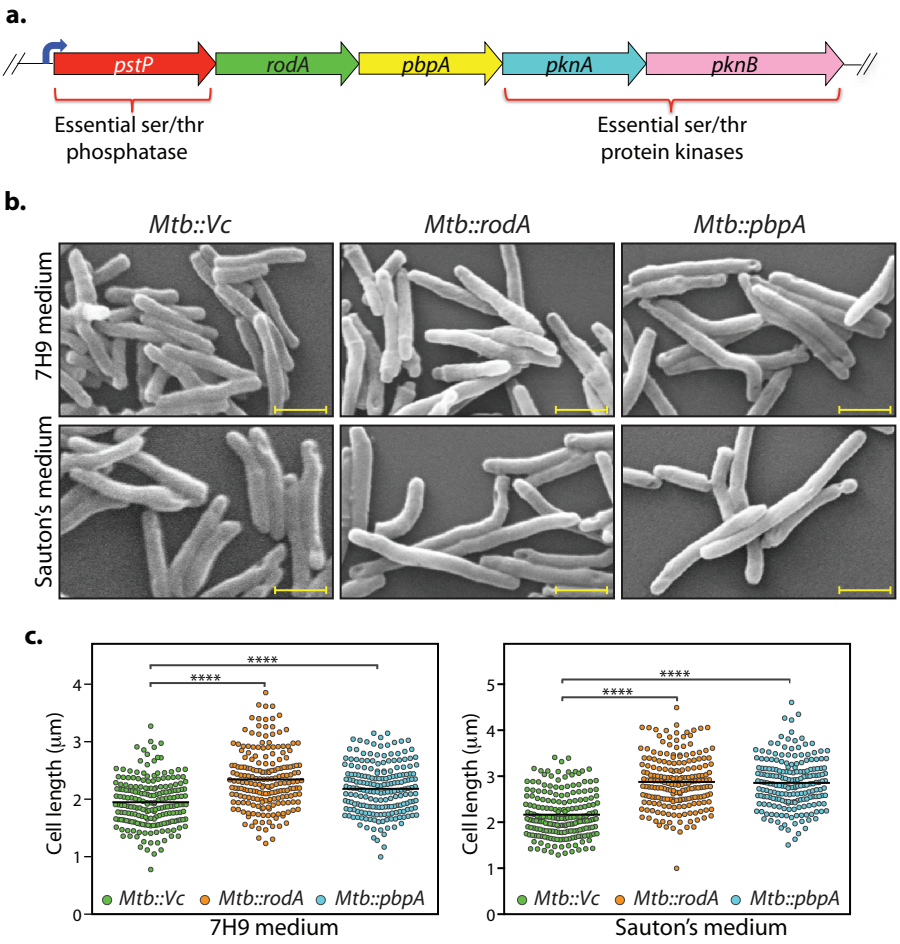
a.
pstP
rodA
pbpA
pknA
pknB
Essential ser/thr phosphatase
Essential ser/thr protein kinases
b.
Mtb::Vc
Mtb::rodA
Mtb::pbpA
7H9 medium
Sauton's medium
c.
Cell length (µm)
****
****
Mtb::Vc
Mtb::rodA
Mtb::pbpA
7H9 medium
Sauton's medium

Figure 3

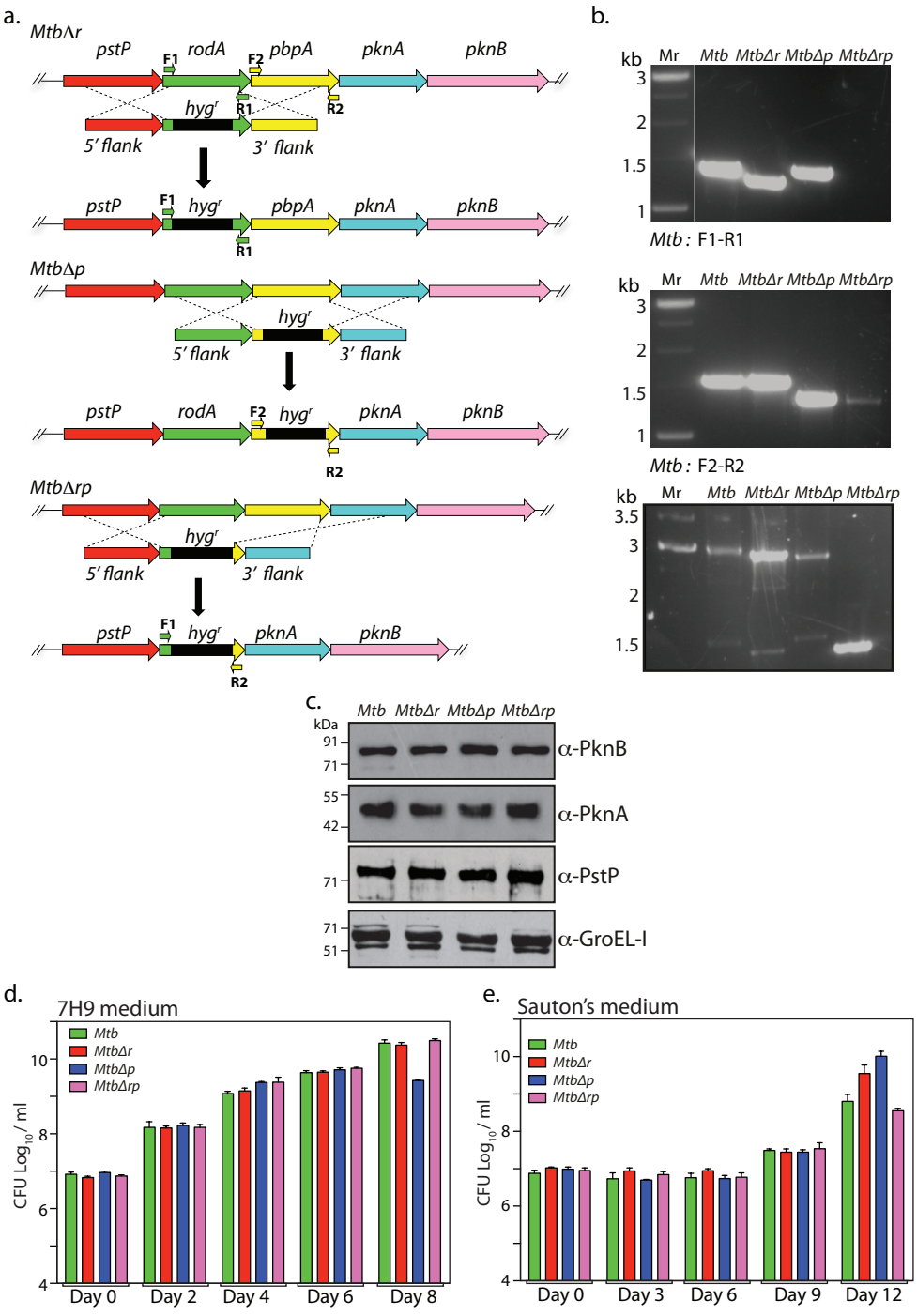
a.
MtbΔr
pstP
rodA
pbpA
pknA
pknB
F1
F2
R1
R2
hygr
5′ flank
3′ flank
MtbΔp
MtbΔrp
b.
kb
Mr
Mtb MtbΔr MtbΔp MtbΔrp
3
2
1.5
1
Mtb : F1-R1
Mtb : F2-R2
3.5
c.
kDa
91
71
55
42
51
α-PknB
α-PknA
α-PstP
α-GroEL-I
d.
7H9 medium
Mtb
MtbΔr
MtbΔp
MtbΔrp
CFU Log10 / ml
10
8
6
4
Day 0
Day 2
Day 4
Day 6
Day 8
e.
Sauton's medium
Day 0
Day 3
Day 6
Day 9
Day 12

Figure 4

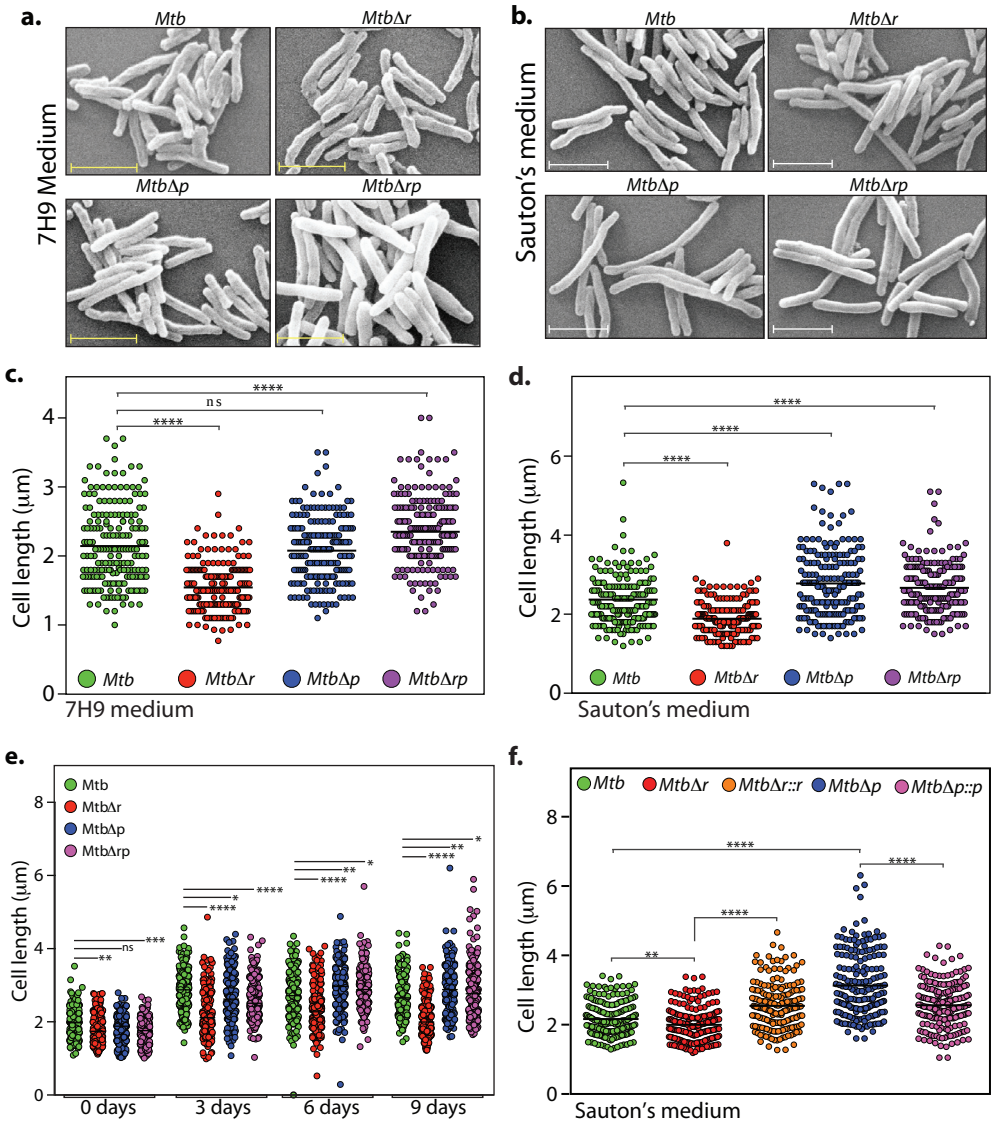
a.
Mtb
MtbΔr
MtbΔp
MtbΔrp
7H9 Medium
b.
Mtb
MtbΔr
MtbΔp
MtbΔrp
Sauton's medium
c.
Cell length (μm)
ns
****
Mtb
MtbΔr
MtbΔp
MtbΔrp
7H9 medium
d.
Cell length (μm)
****
Mtb
MtbΔr
MtbΔp
MtbΔrp
Sauton's medium
e.
Mtb
MtbΔr
MtbΔp
MtbΔrp
Cell length (μm)
ns
0 days
3 days
6 days
9 days
f.
Mtb
MtbΔr
MtbΔr::r
MtbΔp
MtbΔp::p
Cell length (μm)
Sauton's medium

Figure 5

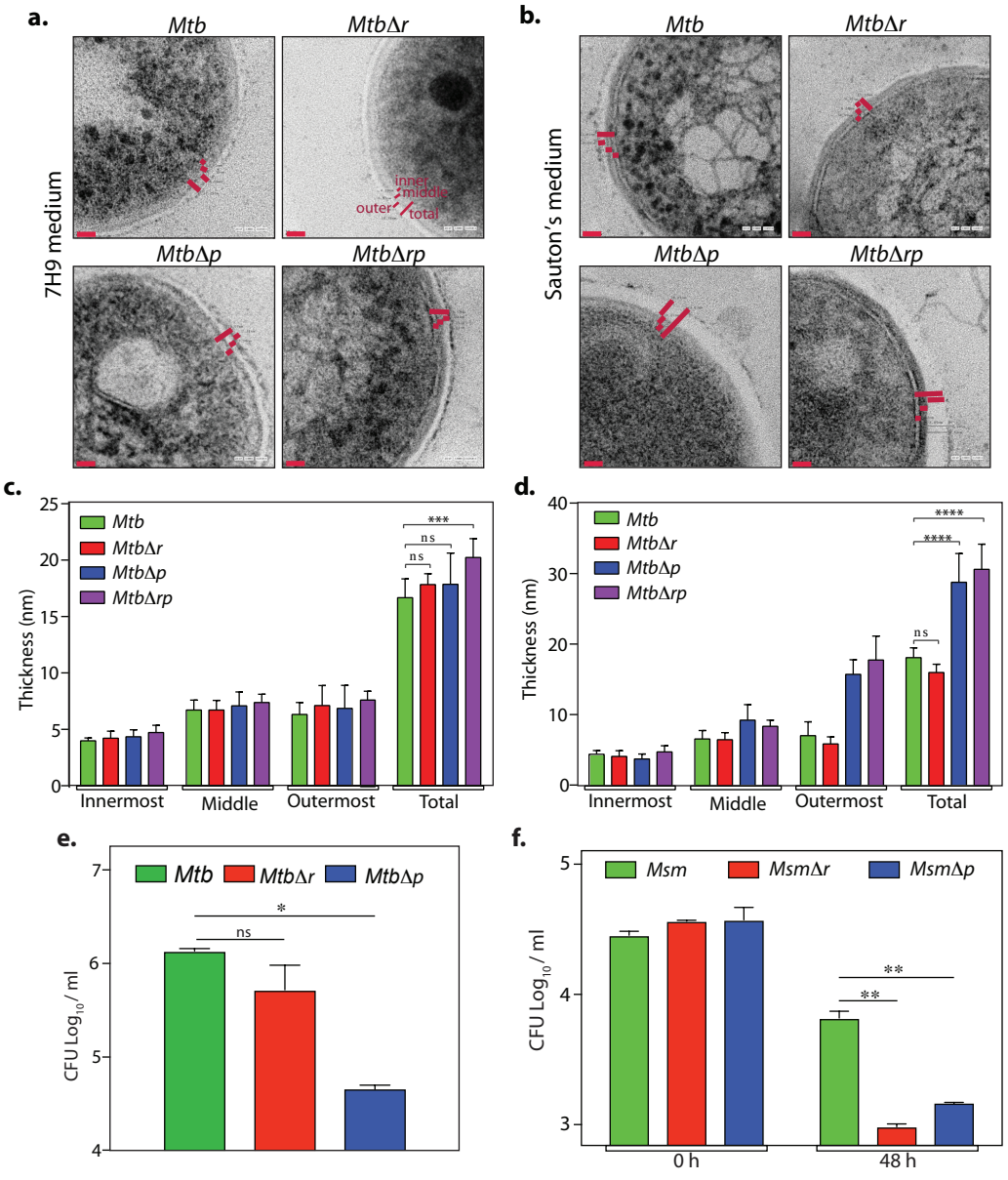
a.
Mtb
MtbΔr
MtbΔp
MtbΔrp
7H9 medium
inner
middle
outer
total
b.
Mtb
MtbΔr
MtbΔp
MtbΔrp
Sauton's medium
c.
Mtb
MtbΔr
MtbΔp
MtbΔrp
Thickness (nm)
Innermost
Middle
Outermost
Total
***
ns
ns
d.
Mtb
MtbΔr
MtbΔp
MtbΔrp
Thickness (nm)
Innermost
Middle
Outermost
Total
****
****
ns
e.
Mtb
MtbΔr
MtbΔp
CFU Log10 / ml
*
ns
f.
Msm
MsmΔr
MsmΔp
CFU Log10 / ml
**
**
0 h
48 h

Figure 6

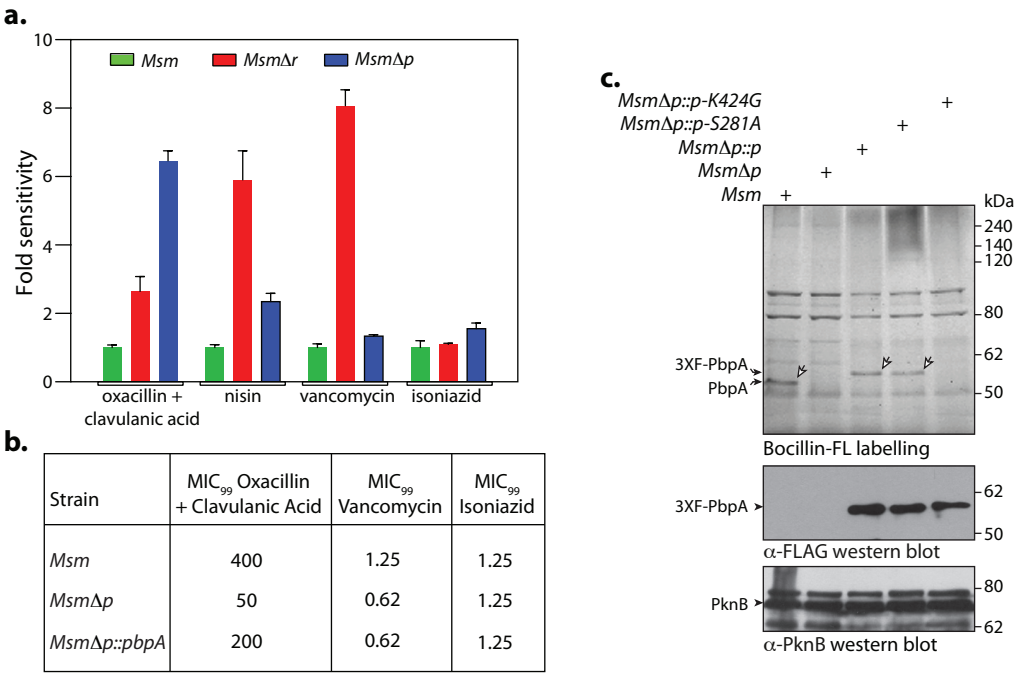

Strain	MIC_{99} Oxacillin + Clavulanic Acid	MIC_{99} Vancomycin	MIC_{99} Isoniazid
Msm	400	1.25	1.25
MsmΔp	50	0.62	1.25
MsmΔp::pbpA	200	0.62	1.25

Figure 7

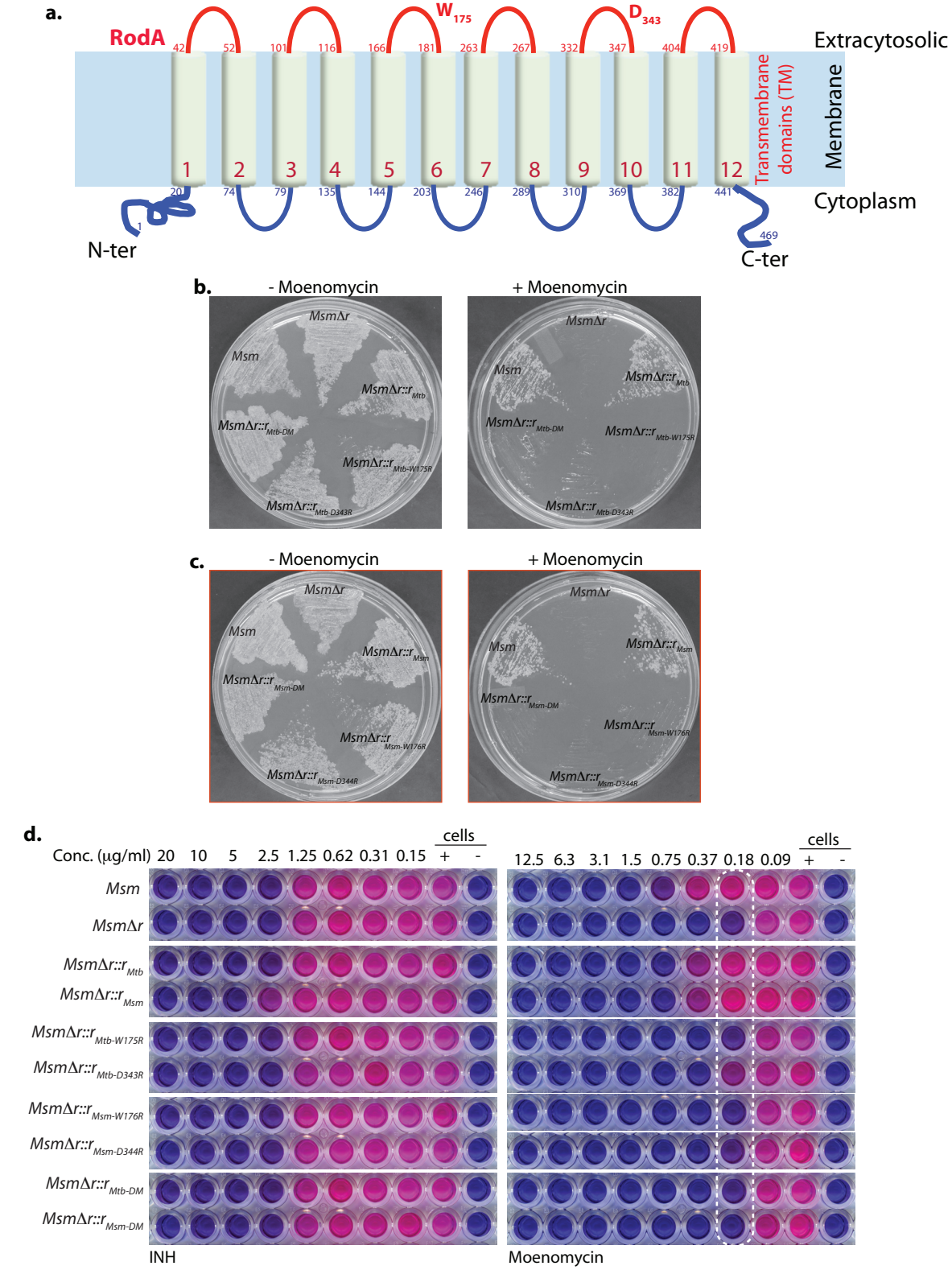
a.
RodA
W175
D343
Extracytosolic
Membrane
Cytoplasm
Transmembrane domains (TM)
N-ter
C-ter
b.
- Moenomycin
+ Moenomycin
c.
- Moenomycin
+ Moenomycin
d.
Conc. (µg/ml) 20 10 5 2.5 1.25 0.62 0.31 0.15
cells + -
12.5 6.3 3.1 1.5 0.75 0.37 0.18 0.09
cells + -
Msm
MsmΔr
MsmΔr::r Mtb
MsmΔr::r Msm
MsmΔr::r Mtb-W175R
MsmΔr::r Mtb-D343R
MsmΔr::r Msm-W176R
MsmΔr::r Msm-D344R
MsmΔr::r Mtb-DM
MsmΔr::r Msm-DM
INH
Moenomycin

Figure 8

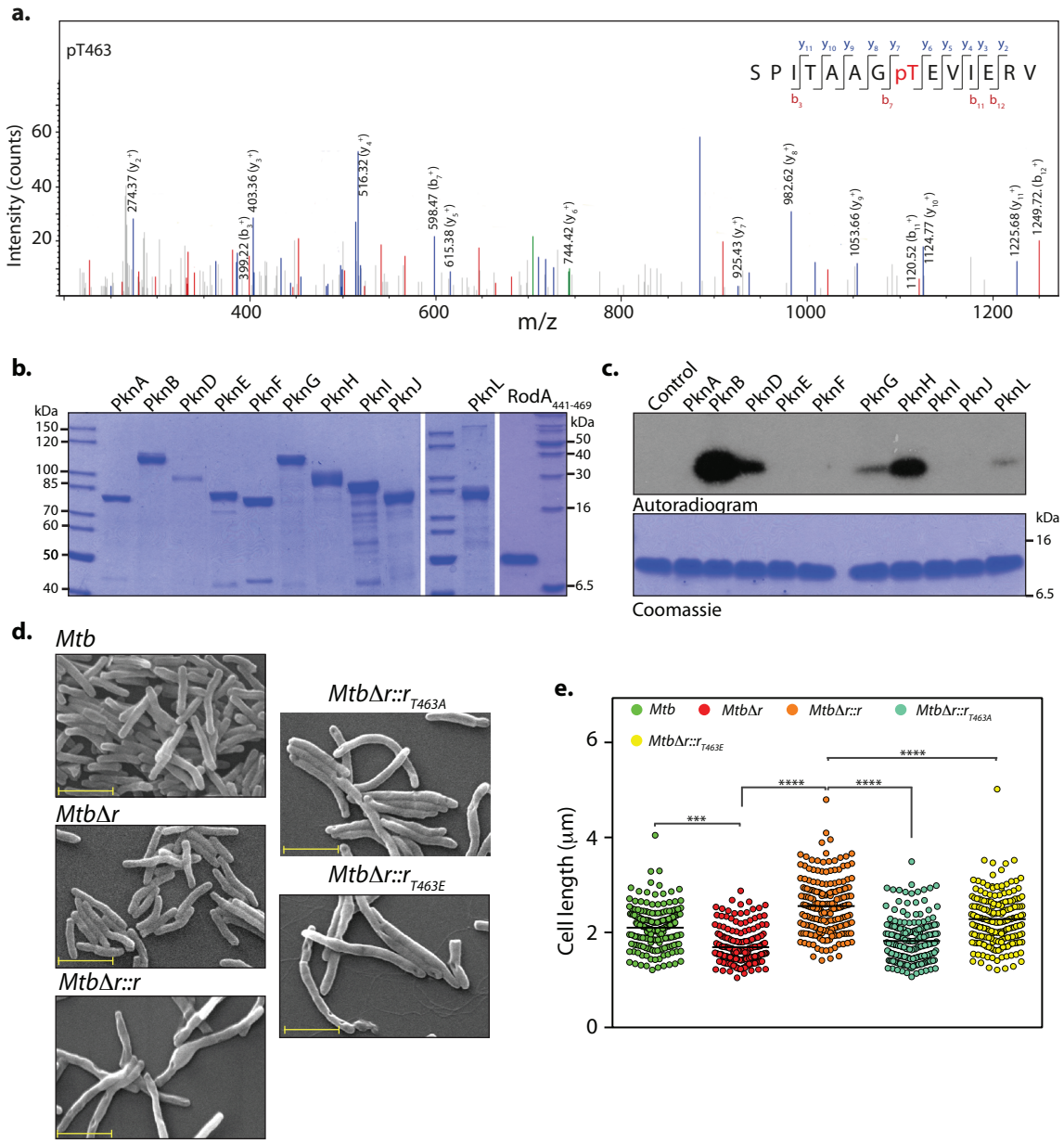
a.
pT463
S P I T A A G pT E V I E R V
Intensity (counts)
m/z
b.
PknA PknB PknD PknE PknF PknG PknH PknI PknJ PknL RodA441-469
kDa
c.
Control PknA PknB PknD PknE PknF PknG PknH PknI PknJ PknL
Autoradiogram
Coomassie
d.
Mtb
MtbΔr
MtbΔr::r
MtbΔr::rT463A
MtbΔr::rT463E
e.
Mtb MtbΔr MtbΔr::r MtbΔr::rT463A MtbΔr::rT463E
Cell length (µm)

Figure 9

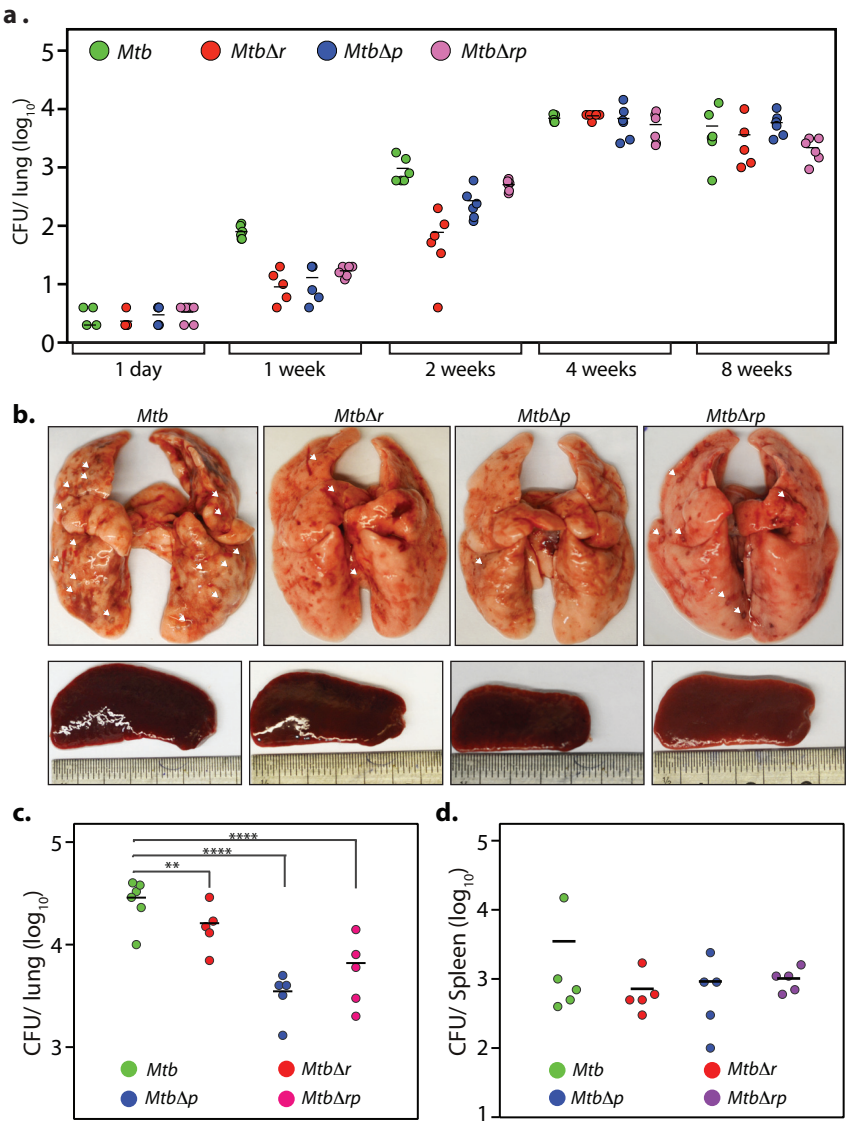
a.
Mtb
MtbΔr
MtbΔp
MtbΔrp
CFU/ lung (log10)
0
1
2
3
4
5
1 day
1 week
2 weeks
4 weeks
8 weeks
b.
Mtb
MtbΔr
MtbΔp
MtbΔrp
c.
CFU/ lung (log10)
****
****
**
Mtb
MtbΔr
MtbΔp
MtbΔrp
d.
CFU/ Spleen (log10)
Mtb
MtbΔr
MtbΔp
MtbΔrp

Figure 10

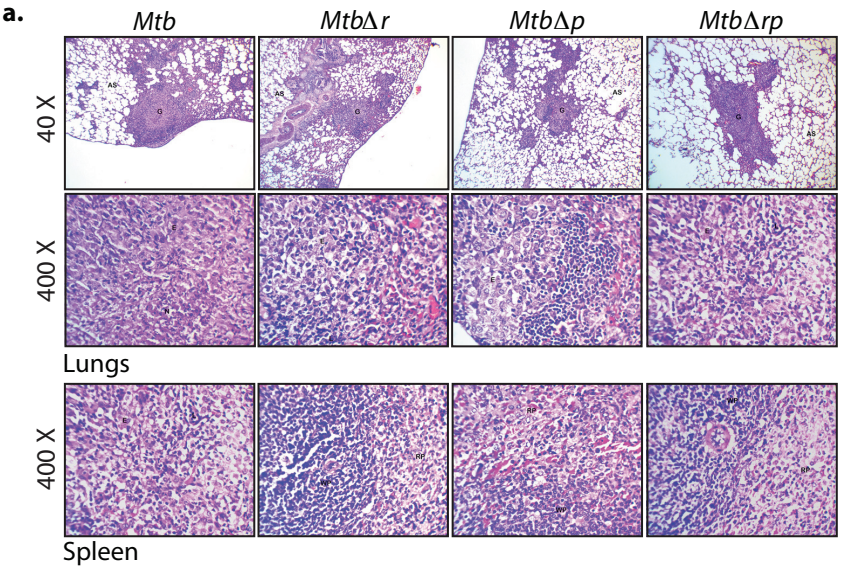

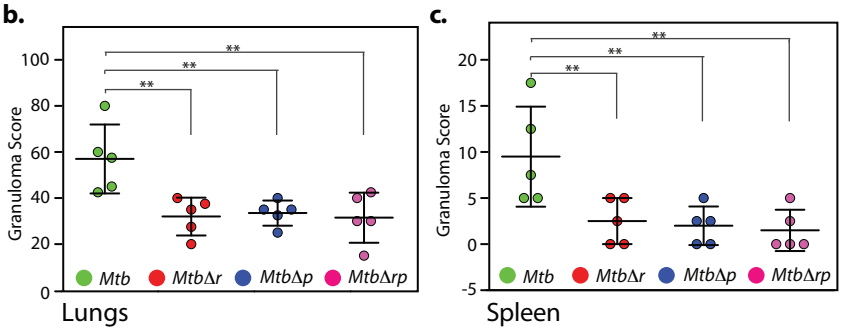

d.

Total granuloma score in the lungs				
Strain	Number of granulomas with Fibrosis Score = 1.0	No Necrosis Score = 2.5	Necrosis Score = 5.0	Total granuloma score
Mtb	0	114	1	290
MtbΔr	0	58	3	160
MtbΔp	0	79	0	167
MtbΔrp	0	67	0	197
Total granuloma score in the spleen				
Strain	Number of granulomas with Fibrosis Score = 1.0	No Necrosis Score = 2.5	Necrosis Score = 5.0	Total granuloma score
Mtb	0	19	1	52.5
MtbΔr	0	5	1	17.5
MtbΔp	0	4	0	10
MtbΔrp	0	3	0	7.5

The transpeptidase PbpA and non-canonical transglycosylase RodA of Mycobacterium tuberculosis play important roles in regulating bacterial cell lengths

Divya Arora, Yogesh Chawla, Basanti Malakar, Archana Singh and Vinay Kumar Nandicoori

J. Biol. Chem. published online March 12, 2018

Access the most updated version of this article at doi: 10.1074/jbc.M117.811190

Alerts:
- When this article is cited
- When a correction for this article is posted

Click here to choose from all of JBC's e-mail alerts

Downloaded from http://www.jbc.org/ by guest on March 31, 2018